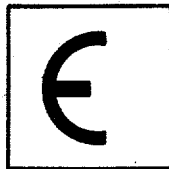


Commission of the European Community

JOINT
RESEARCH
CENTRE



NEANDC (E) 222 "U" Vol. III Euratom
INDC (EUR) 014/G

ANNUAL PROGRESS REPORT ON NUCLEAR DATA

1980

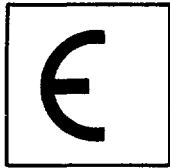
CENTRAL BUREAU FOR NUCLEAR MEASUREMENTS

GEEL (BELGIUM)

March 1981

Commission of the European Community

JOINT
RESEARCH
CENTRE



NEANDC (E) 222 "U" Vol. III Euratom

INDC (EUR) 014/G

ANNUAL PROGRESS REPORT ON NUCLEAR DATA

1980

CENTRAL BUREAU FOR NUCLEAR MEASUREMENTS

GEEL (BELGIUM)

March 1981

TABLE OF CONTENTS

	<u>PAGE</u>
NUCLEAR DATA	3
1. <u>NEUTRON DATA</u>	3
1.1. Cross Sections of Actinides	3
1.2. Cross Sections of Structural Materials	11
1.3. Cross Sections of Fission Products	14
1.4. Gas Producing Reactions	14
1.5. Various Measurements	19
1.6. Standard Neutron Data	27
1.7. Evaluation and Underlying Physics	31
1.8. Major Research Equipment	35
2. <u>NON-NEUTRON NUCLEAR DATA</u>	40
2.1. Decay Studies	40
2.2. Half-life Determinations	48
2.3. Compilations and Evaluations	50
2.4. Satellite Peaks in High Resolution Alpha Spectrometry and their Use in Determining the Energy Loss of Recoiling Nuclei of the ^{228}Th Series to Electronic Processes in Silicon	51
2.5. Improvement of Measurement and Source Preparation Techniques	53
2.6. Programme-linked Activities	58
LIST OF PUBLICATIONS	61
CINDA ENTRIES	64

N U C L E A R D A T A

1. NEUTRON DATA

1.1 Cross Sections of Actinides

Fission cross section of ^{233}U and ^{241}Pu

C. Wagemans^{*}, R. Barthélémy, J. Van Gils^{*}

A new series of fission cross section measurements are being performed at GELINA, using surface barrier detectors and back-to-back fission and ^{10}B foils. The aim of these experiments is to cover the neutron energy range from thermal up to 100 keV in one single measurement. Substantial progress has been made in this respect and results from a first run are being analysed.

Measurement of neutron induced capture cross section and α of ^{235}U between 1 and 100 keV

L. Calabretta^{**}, F. Corvi, M. Merla, M.S. Moore^{***}, T. van der Veen

A measurement of capture and α for ^{235}U was performed using four C_6F_6 liquid scintillators each of 10.2 cm diameter and 7.6 cm height, which surrounded the sample, consisting of a multiplate fission chamber (21 plates, U_3O_8 coated, ^{235}U enriched) containing about 2.5 g of ^{235}U .

In the final experimental set up, the linac was operated at maximum power (10 kW) and the detector system was placed at 28 m distance, yielding a time of flight resolution of 0.5 nsec/m.

The pulses of the C_6F_6 detectors in coincidence with the fission chamber were considered as fission γ -rays while the others belong either to capture γ -rays or to γ -rays from undetected fissions. The pulses were weighted according to their amplitude in order to achieve a response proportional to the total γ -ray energy.

The accuracy of the measurement with a low signal to background ratio (typically one to one or worse) depends mainly on the background determination. Therefore an aluminium "black resonance" filter (2.5 cm thick) was permanently kept in the neutron beam in order to monitor the background at 35 and 88 keV.

^{*} SCK/CEN, Mol, Belgium
^{**} Bursary of the European Community
^{***} Visiting scientist from LASL

The detailed shape of the background was then determined by measuring with a mock chamber containing the same amount of aluminium as the fission chamber. The neutron flux was measured with a thin Li glass detector (0.5 mm thick) in transmission. The absolute normalisation was performed with a 0.6 mm thick gold sample.

Fig. 1.1 displays the anti-coincidence yield of foreground and of background normalised to the same value in the dip of the 35 keV black resonance.

Another background to be subtracted consists of fission γ -rays and in coincidence with fission chamber pulses. This was evaluated by measuring the efficiency of the chamber in two independent ways:

i) by measuring the coincidence rate between the fission chamber exposed to a thermal neutron flux, and a fast neutron detector consisting of a NE 213 liquid scintillator coupled to a pulse shape discrimination circuit. If

the fast neutrons present are

only produced from fissions in the chamber, then the ratio of coincidences to single rate in the neutron detector yields the efficiency. A value of $\epsilon = 0.839$ was found;

ii) by performing a run at thermal neutron energy in which the ^{235}U capture rate was compared to that of an Au sample. From this comparison and the known thermal cross sections the amount of undetected fissions and hence the efficiency was derived: a value $\epsilon = 0.833$ was found.

The average of the 2 determinations $\bar{\epsilon} = 0.836 \pm 0.02$ was adopted in the analysis. The same thermal run described above was used to calibrate α : the analysis was then extended up to the epithermal region yielding α -values for 15 well resolved resonances in the range 3-40 eV.

These values are in overall agreement with the ENDF/B-V resonance parameters. Values of α in the unresolved region are plotted in Fig. 1.2 together with

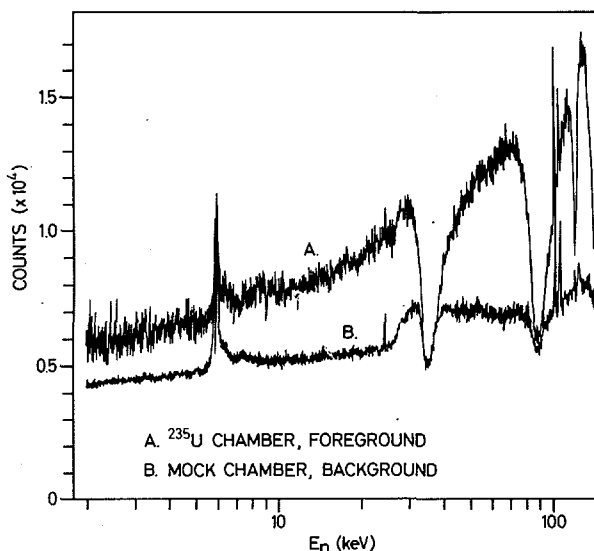


Figure 1.1 Capture detectors counts not in coincidence with fission chamber pulses.

those of Gwin et al.⁽¹⁾ and Muradyan et al.⁽²⁾.

Our data seem to be in excellent agreement with this last work.

Fission fragment mass- and energy-distributions for the neutron induced fission of ^{235}U and ^{239}Pu as a function of the spin of the resonances

C. Wagemans^{*}, H. Weigmann,
G. Wegener Penning^{*}, R. Barthélémy

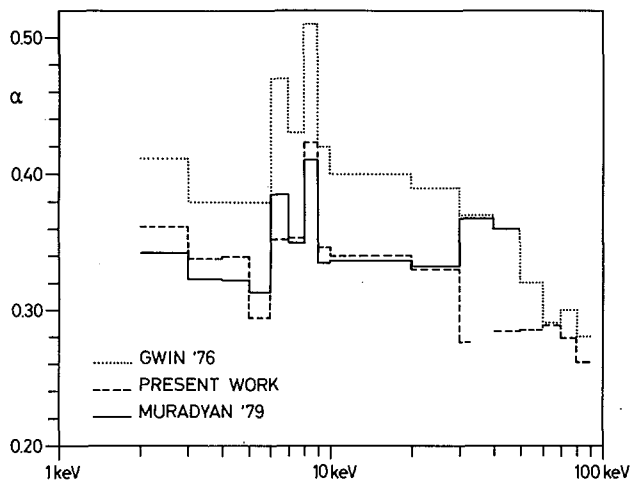


Figure 1.2 α of ^{235}U in the range 2-90 keV.

The data acquisition system has been strongly improved: EMI magnetic tape unit has been replaced by a HP 1000 computer with an IBM compatible magnetic tape unit. With this apparatus the pulse-heights of the coincident fission fragments are recorded in 1024 x 1024 channels for 4096 different neutron energies simultaneously. At present the system is being calibrated with the well-known thermal fission of ^{235}U . The results are very satisfactory. In addition, a measurement of the $^{235}\text{U}(n,f)$ -fragment mass- and energy-distribution has been performed in the neutron energy region below 1 eV. These results are being analysed.

Fission cross section of ^{238}Pu

H.-H. Knitter, C. Budtz-Jørgensen, D.L. Smith^{**}, H. Bax, R. Vogt

^{238}Pu has an alpha half-life of only 87.75 y and a spontaneous fission half-life of $4.77 \cdot 10^{10}$ y. These properties make it difficult to measure the neutron induced fission cross section of ^{238}Pu . A fission ionization chamber with good discrimination between fission fragments and alphas was used for the measurements. The fission cross-section was measured in a back-to-back geometry relative to the ^{235}U standard fission cross section, using the 7 MV Van de Graaff accelerator as a pulsed neutron source. The neutron energy range covered by this experiment extends from 200 keV to 10 MeV using the

(1) R. Gwin et al., Nucl. Sci. Eng. 59, 79 (1976)

(2) G.V. Muradyan et al., Proc. Int. Conf. on Nuclear Cross Sections for Technology, Knoxville 1979, p. 488

^{*} SCK-CEN, Mol, Belgium
^{**} Visiting scientist from ANL

neutron source reactions ${}^7\text{Li}(p,n){}^7\text{Be}$, $\text{T}(p,n){}^3\text{He}$ and $\text{D}(d,n){}^3\text{He}$ in their appropriate ranges.

Due to the short half-life of ${}^{238}\text{Pu}$ a sample of only $47.7 \mu\text{g}$ ${}^{238}\text{Pu}$ could be used in the present measurements. This amount gives an alpha activity of $3 \cdot 10^7 \text{ s}^{-1}$. In spite of this high alpha rate the fission chamber allows a measurement of the fission fragments with a detection efficiency of 96 %. Fig. 1.1.3A shows a fission fragment spectrum and Fig. 1.1.3B the same spectrum with alpha-background subtracted. Some 80 cross section points were measured in the entire neutron energy range.

The evaluation of the raw experimental data has started. The fission chamber will now be positioned at a 8 m flight-path station of the Linac to extend the measurements towards the low energy region.

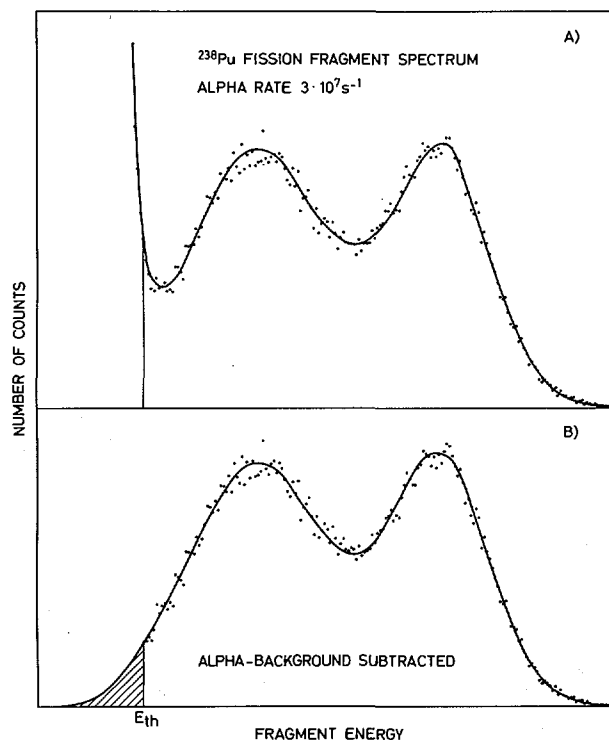


Figure 1.3 Fission fragment energy spectrum of ${}^{238}\text{Pu}$ measured at the Van de Graaff in the presence of $3 \cdot 10^7$ alphas s^{-1} . Part A) shows the full spectrum, in part B) the alpha background is subtracted. The fission fragment detection efficiency is 96 %.

Fission cross section of ${}^{239}\text{Pu}$

C. Wagemans^{*}, G. Coddens^{*}, H. Weigmann, J.A. Wartena, R. Barthélémy

A paper entitled: "Measurement of the ${}^{239}\text{Pu}(n,f)$ cross-section from thermal up to 30 keV neutron energy" was published in Annals of Nuclear Energy, Vol.7, N° 9, pp. 495-503 with the following abstract:

" At GELINA measurements of the ${}^{239}\text{Pu}$ fission cross-section were performed covering the neutron energy region from thermal up to 30 keV. Fission fragment as well as fission neutron detection techniques were used. Also for the neutron flux determination different methods were applied. From the σ_f -data, several fission integrals were calculated and compared with other results".

^{*} SCK-CEN, Mol, Belgium

Neutron induced fission cross section of ^{240}Pu in the energy range from 10 keV to 10 MeV

C. Budtz-Jørgensen, H.-H. Knitter

This work has been finalized. A manuscript under the above-mentioned title and with the following abstract has been accepted by the journal Nuclear Science and Engineering:

" The neutron induced fission cross section of ^{240}Pu was measured in the neutron energy range from 10 keV to 10 MeV using the 7 MV Van de Graaff and the electron linear accelerator of the CBNM as pulsed neutron sources, which delivered monoenergetic and continuous neutron spectra respectively. The neutron induced fission events were detected with a parallel plate ionization chamber which provides a fast and narrow output signal allowing ns-timing, but where the time integral of the pulse contains at the same time the energy information of the ionization particle. This detector permits a high discrimination between alpha particles and fission fragments at an alpha rate of some 10^7s^{-1} . The fission cross section data below 400 keV are especially remarkable since they were taken with an energy resolution almost one order of magnitude better than any other published data set. In this region large structures in the fission cross section due to class II states in the second well of the double-humped fission barrier were found. The spontaneous fission half life of ^{240}Pu was measured also."

Fission barriers and fission probabilities of ^{241}Pu and ^{240}Pu

H.-H. Knitter, C. Budtz-Jørgensen

The measured neutron induced fission cross section of ^{240}Pu in the energy range up to 10 MeV covers the regions of the first and second chance fission thresholds. Therefore in principle an analysis of the fission cross section in this energy range allows the evaluation of the fission barriers of ^{241}Pu and ^{240}Pu . The same physical model as applied for the determination of the ^{242}Am fission barriers was used to obtain the parameters of the double humped fission barrier of ^{241}Pu . The level density formulas of Jensen and Sandberg⁽¹⁾, as modified by Jensen⁽²⁾ for low excitation energies, were adjusted such that they reproduce the observed ones at the neutron binding energy. Neutron transmission coefficients, the spin distribution of the compound nucleus and the compound formation cross section were obtained from optical model calculations. The results of this evaluation are $V_A = 6.04 \pm 0.05$ MeV, $\hbar\omega_A = 0.55 \pm 0.05$ MeV, $V_B = 5.56 \pm 0.20$ MeV, where V_A , $\hbar\omega_A$ represent the height and curvature of the

(1) A.S. Jensen, J. Sandberg, Physica Scripta 17, 107 (1978)

(2) A.S. Jensen, Proc. Intern. Conf. on Neutron Physics and Nuclear Data, Harwell 1978, p. 378

inner barrier and V_B the height of the outer barrier. $\hbar\omega_B$ was fixed at 0.52 MeV, since its value was not very sensitive with respect to the fission cross section. A comparison with fission barrier parameters obtained by Back et al. (1) from $^{239}\text{Pu}(t, pf)$ measurements, shows a large difference in the width of the first barrier of ^{241}Pu . This becomes evident also from a direct comparison of the measured fission probabilities of the two experiments as can be seen in Fig. 1.4.

The cross section in the region of the second chance fission due to the $^{240}\text{Pu}(n, n'f)$ process has been calculated also, using the double-humped fission barrier parameters of ^{240}Pu as obtained by Goldstone et al. (2) from $^{239}\text{Pu}(d, pf)$ measurements. Proper population distributions of levels of ^{240}Pu due to the energy and angular momentum distribution of the inelastically scattered neutron were taken into account. The results are shown as a dashed line in Fig. 1.5.

Also here the level densities were normalized to observed values at the neutron binding energy. The rise of the fission probability becomes too steep compared with the experiment, because the fission probability approached rapidly the value one in the excitation energy region of ^{240}Pu above the fission barrier and below the neutron binding energy. It was not possible to describe the fission cross section with the present model using level densities which are near to those observed at the neutron binding energy as well as fission barrier parameters near to those published in the literature.

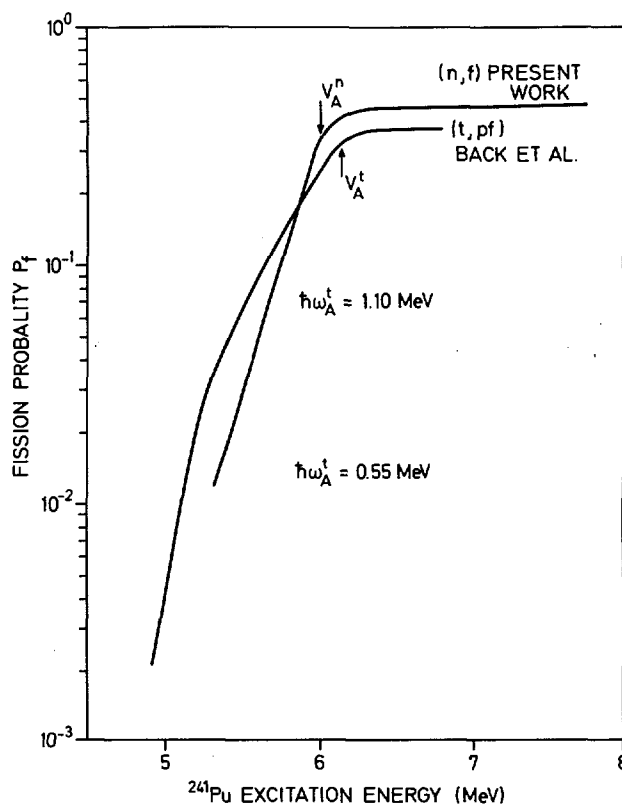


Figure 1.4 The experimental fission probabilities obtained by Back et al. from $^{239}\text{Pu}(t, pf)$ and by the present $^{240}\text{Pu}(n, f)$ measurements are plotted versus the excitation energy of ^{241}Pu .

-
- (1) B.B. Back et al., Proc. Symp. on Physics and Chemistry of Fission, Rochester 1073, p. 3
 (2) P.D. Goldstone et al., Phys. Rev. C18, 1706 (1978)

One can however reproduce the measured cross section using a much larger radiative width than observed. This can be seen from the full and dotted line in Fig. 1.5. We think that the model has to be more elaborated and in a next step a model using three barriers, with the third barrier parallel to the outer one will be tried.

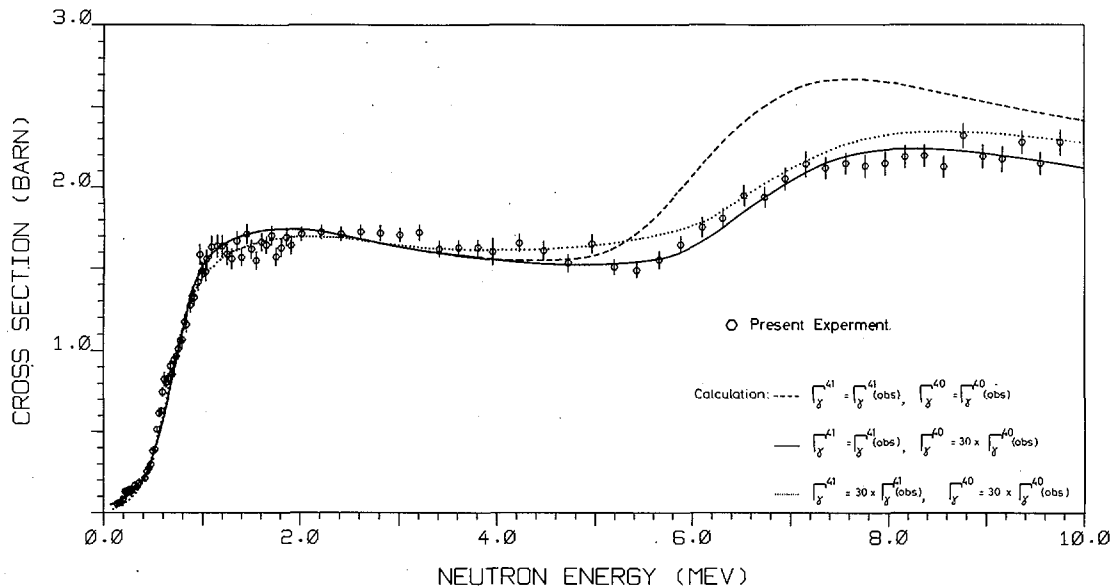


Figure 1.5 The neutron induced fission cross section is plotted versus the incident neutron energy. The hexagons are the present measurements. The dashed line represents calculations using level density formulas adjusted to those observed at an excitation energy equal to the neutron binding energies, fission barrier parameters of ^{241}Pu equal to those which describe the threshold behaviour of the $^{240}\text{Pu}(n,f)$ reaction and the ^{240}Pu fission barrier parameters as obtained by Goldstone et al.

Fission fragment mass- and energy-distributions for the neutron induced fission of ^{241}Pu and the spontaneous fission of ^{242}Pu

E. Allaert^{*}, C. Wagemans^{*}, G. Wegener-Penning^{*}, A. Deruytter, R. Barthélémy

The spontaneous fission of ^{242}Pu was studied during the annual shut-down of GELINA. For calibration and comparison purposes, a measurement of the thermal neutron induced fission of ^{241}Pu was performed before and after the $^{242}\text{Pu}(s.f.)$ measurement. In order to keep the experimental conditions almost identical for both measurements, a combined $^{241}\text{Pu} - ^{242}\text{Pu}$ target was used, containing about equal amounts of ^{241}Pu and ^{242}Pu . A partial analysis of the

^{*} SCK-CEN, Mol, Belgium

data reveals a drastic difference in shape for the $^{242}\text{Pu}(\text{s.f.})$ and the $^{241}\text{Pu}(n_{\text{th}},\text{f})$ mass-distributions. Moreover, the total kinetic energy of the fission fragments is higher for $^{242}\text{Pu}(\text{s.f.})$ than for $^{241}\text{Pu}(n_{\text{th}},\text{f})$, quite opposite to analogous results obtained for the fissioning system ^{240}Pu (1). The measurements are continuing.

Fission cross sections of ^{242}Pu and ^{244}Pu

M.S. Moore^{*}, J.A. Wartena, H. Weigmann, C. Budtz-Jørgensen, H.-H. Knitter

Measurements of the fission cross sections on samples of ^{242}Pu (160 mg) and ^{244}Pu (40 mg), supplied by LASL, have been finished. Analysis of the data is under way. Since the ^{242}Pu sample contained about 7 % of ^{239}Pu the analysis of the data obtained from this sample will be limited to the threshold region and above ($\sim 0.5 \text{ MeV} < E_n < \sim 5 \text{ MeV}$).

For ^{244}Pu also the subthreshold region, where the data show a number of narrow isolated resonances, will be analysed. Measurements on the fission fragment angular distribution will be started soon for ^{244}Pu .

Neutron Capture Cross Section of ^{241}Am

E. Cornelis^{***}, L. Mewissen^{**}, J. Vanpraet^{***}, J.A. Wartena, S. Raman^{****}

Analysis of the second set of our absorption cross-section data has been continued.

Capture events were weighted according to their measured pulse height for achieving a detector output proportional to the gamma-ray energy released in the capture event. A typical weighted time-of-flight spectrum is shown in Fig. 1.6.

The energy dependence of the neutron flux was measured with

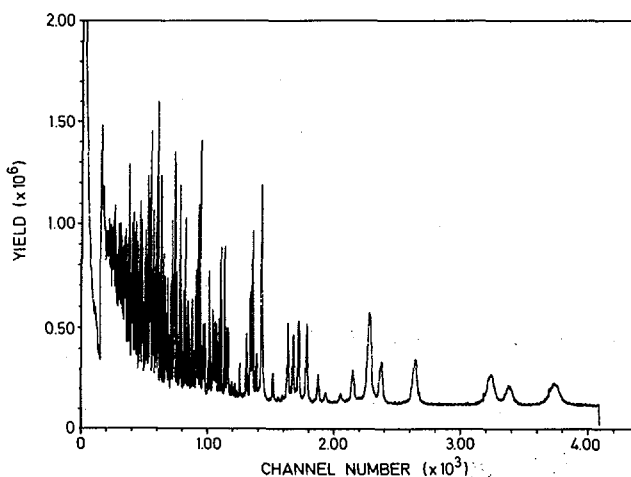


Figure 1.6 Time-of-flight spectrum of ^{241}Am .

(1) C. Wagemans, G. Wegener-Penning, H. Weigmann, R. Barthél my, Proc. Conf. on Phys. and Chem. of Fission, IAEA, Vienna (1980) 143

^{*} Visiting scientist from LASL
^{**} SCK-CEN, Mol, Belgium
^{***} Rijksuniversitair Centrum, Antwerpen, Belgium
^{****} Visiting scientist from ORNL

an avalanche detector using ^{10}B and ^{235}U .

Typical yields are plotted as a function of time (channel-number) in Fig. 1.7 A and B. The background fit was obtained by means of the black resonance technique using S, Na, Co and Au. The shape of the $^{241}\text{Am}(n,\gamma)$ cross sections versus energy will be derived after determining a suitable function to describe the neutron flux in the energy region from about 5 eV up to 100 keV.

1.2 Cross Sections of Structural Materials

Measurement of (n,a) cross sections on Cr, Fe and Ni in the 5 to 10 MeV energy range

A. Paulsen, H. Liskien,
F. Arnotte, R. Widera

The measurements on iron and nickel were supplemented by those on chromium.

All results and a detailed description of the measurements are given in a paper which was submitted to the journal Nuclear Science and Engineering. It is entitled: "Measurement of (n,a) cross-sections on Cr, Fe and Ni in the 5 to 10 MeV neutron energy range". It has the following abstract:

" A measuring programme has been carried out at the CBNM Van de Graaff accelerator facility for the determination of (n,a) cross sections on the main constituents of fast reactor structural materials, namely the elements chromium, iron and nickel. The a particles are detected in a reaction chamber by telescope counter arrangements at five observation angles between 14 and 141°. Results obtained in the energy-range from 5 to 10 MeV are presented in terms of laboratory angle-differential cross sections, relative Legendre polynomial coefficients of angular distributions, angle-integrated cross sections and average a-energies."

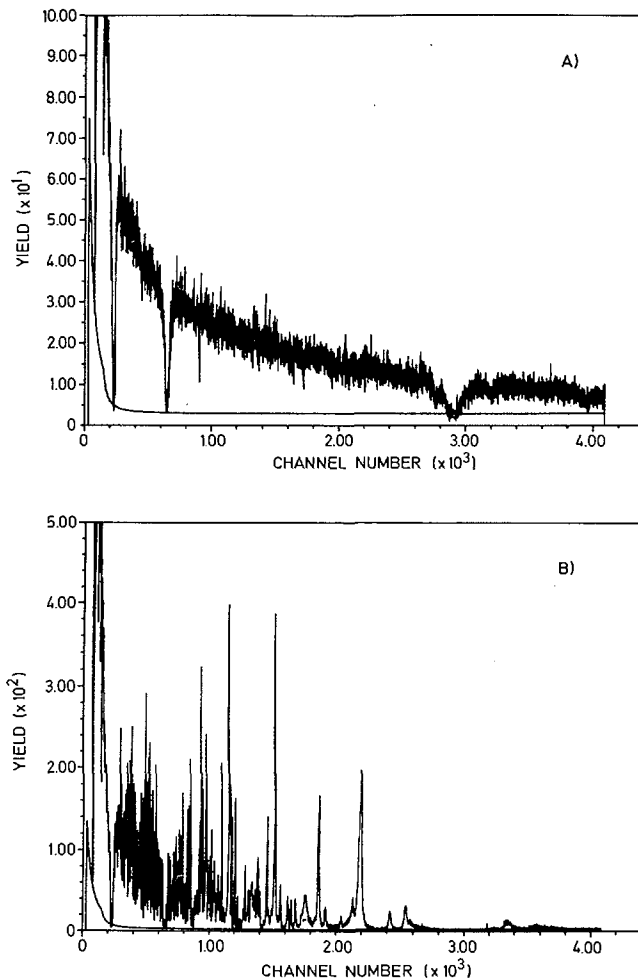


Figure 1.7 Avalanche detector yield with background fit. A) ^{10}B and B) ^{235}U .

High resolution neutron capture cross sections of Fe and Cr isotopes

B.J. Allen^{*}, A. Brusegan, F. Corvi, G. Rohr, R. Shelley

High resolution capture cross-section measurements of the iron and chromium isotopes have continued with enriched samples of ^{54}Fe and ^{52}Cr on loan from ORNL. The oxide samples were packed in 0.3 mm thick aluminium containers of 8 cm diameter, and at a neutron flight-path of 60 m. Neutron capture γ -rays were detected with two deuterated benzene (C_6D_6) detectors and off-line pulse-height weighting of detected γ -rays was used to ensure that the capture efficiency was independent of the resonance γ -ray spectra. The linac was operated at 800 Hz with a pulse width of 4 ns.

Neutron flux measurements were done with a 0.5 mm ^6Li glass in the transmission mode, and with a boron slab viewed by two C_6D_6 detectors. The absolute normalization of the data was obtained by means of the 1.15 keV resonance in ^{56}Fe , the resonance parameters of which were determined by accurate transmission measurements.

The ^{54}Fe and ^{52}Cr data are of better quality than earlier measurements at ORELA ⁽¹⁾ in that the sensitivity of the detector-system to resonance scattered neutrons is much reduced, and the flight-path used at the Linac is 50 % longer. Although the sensitivity of the Linac capture system has not yet been investigated in detail, a lower effect is expected because of the absence of fluorine in the scintillator. Measurements of the neutron sensitivity are planned by observing γ -ray yields from resonances in Al and Si with large neutron scattering widths.

A striking feature of the ^{54}Fe data is the asymmetry observed in the s-wave resonances at 99, 130, 147, 174 and 190 keV. Pending clarification of the role of the neutron sensitivity these results support the observation of asymmetries reported by Allen et al. (1978)⁽²⁾ for the ORELA data which were interpreted as interference between the single particle or valence components of s-wave resonances with large neutron widths. The effect is so significant that a multi-level multi-capture channel analysis will be required.

At present analysis of the ^{54}Fe data is proceeding using both area (TACASI) and shape (FANAC) fitting programmes for the determination of resonance capture widths. The latter code, based on a R-matrix calculation of the

(1) B.J. Allen, A.R. de L. Musgrove, J.W. Boldeman, R.L. Macklin, Nucl. Phys. A283, 37 (1977)

(2) B.J. Allen, A.R. de L. Musgrove, W.K. Bertram, Phys. Lett. 72B, 323 (1978)

* Visiting scientist from AAEC Lucas Heights

scattering cross-section, has recently been adapted to the high resolution requirements of the Linac measurements.

Both programmes include Doppler and resolution broadening and calculate the multiple scattering correction.

Total neutron cross section measurements on Fe and Cr isotopes

Measurements in the energy range from 0.5 keV up to 150 keV

A. Brusegan, A. Dufraşne

Previous total cross section measurements on natural Cr and Fe samples were followed by transmission measurements on isotopically enriched material of ^{50}Cr , ^{52}Cr , ^{53}Cr and ^{57}Fe on loan from ORNL. Samples were packed in aluminium containers of 8 cm diameter. The detection system, placed at about 49 m, consists of 2 NaI(Tl) detectors viewing a 0.3 cm thick sintered boroncarbide slab. The Linac running parameters were: 4 ns burst width, 800 Hz at 100 MeV electron energy. The background, always below 3 %, was determined with the "black resonance" technique using S, Na and Bi filters and was mainly depending on the direct neutron beam. For this reason the dependence of the background on the beam attenuation was measured.

For transmission measurements resonance parameters ⁽¹⁾ have, up to now, been determined only for the 1.15 keV resonance in ^{56}Fe analysing the data taken with the natural iron samples.

High resolution measurements in the range from 35 keV to 19 MeV

E. Cornelis^{***}, C.R. Jungmann^{**}, L. Mewissen^{*}, F. Poortmans^{*}

We have completed the transmission experiments on the enriched isotopes (on loan from ORNL) of ^{50}Cr , ^{52}Cr , ^{53}Cr , ^{54}Fe , ^{56}Fe , ^{57}Fe in the energy-range from 35 keV up to 19 MeV. The experiments were performed on a 200 meter flight-path, using the moderated neutron beam from the Gelina neutron target in the energy range from 35 keV up to 500 keV. A 400 meter flight-path and unmoderated neutron beam was used for experiments between 300 keV and 19 MeV. Data reduction and analysis has started.

(1) A. Brusegan, F. Corvi, G. Rohr, R. Shelley, T. van der Veen, Proc. Int. Conf. of Nucl. Cross Sections and Technology, University of Tennessee, Knoxville, U.S.A., October 22-26, 1979, NBS Special Publication 594, 163

* SCK-CEN, Mol, Belgium

** Bursary of the European Community

*** Rijksuniversitair Centrum, Antwerpen, Belgium

1.3 Cross Sections of Fission Products

Cross section measurements for the reaction $^{103}\text{Rh}(n,n')^{103m}\text{Rh}$

A. Paulsen, R. Widera, R. Vaninbroukx, H. Liskien

A paper appeared under the above title in Nuclear Science and Engineering 76 (1980) 263. The abstract is as follows:

" The excitation function for the reaction $^{103}\text{Rh}(n,n')^{103m}\text{Rh}$ was measured by the activation technique from 0.2 to 6.1 MeV in 0.1-MeV steps and from 13.0 to 16.7 MeV in 1-MeV steps. This excitation function is normalized through an absolute measurement at 1.8 MeV. This measurement is based on n-p scattering for neutron flux determination and on liquid scintillation counting of ^{103m}Rh separated from ^{103}Pd solutions for the activity determination. The total uncertainty of the cross-section results is typically + 5 % above 0.5 MeV (about + 10 % above 13 MeV). Concurrence with existing data is good except below 0.35 MeV, where the present results are considerably higher."

Present results and their comparison to existing data are given in Fig. 1.8.

Resonance Parameters of Pd isotopes

P. Staveloz^{**}, E. Cornelis^{***}, L. Mewissen^{*}, F. Poortmans^{*}, G. Rohr, R. Shelley, T. van der Veen

Resonance-parameter analysis of all data (capture, transmission, scattering and parity assignments) for the isotopes $^{104,105,106,108,110}\text{Pd}$ is completed. From these results, the average and statistical properties of the resonance parameters (strength functions, s-wave level spacings and average capture widths) will be deduced.

1.4 Gas Production Reactions

Tritium Breeding from ^7Li

H. Liskien, A. Paulsen

Recent results from AERE Harwell (1) on the $^7\text{Li}(n,t)$ cross section are systematically 25 % lower than presently used ENDF/B-IV values. Such low values would cause serious changes in present concepts for blankets design of fusion reactors.

(1) M.T. Swinhoe, C.A. Uttley, Proc. Int. Conf. on Nuclear Cross Sections and Technology, University of Tennessee, Knoxville, USA, October 22-26, 1979 NBS Special Publication 594, 246

* SCK-CEN, Mol, Belgium
** Bursary of the European Community
*** Rijksuniversitair Centrum, Antwerpen, Belgium

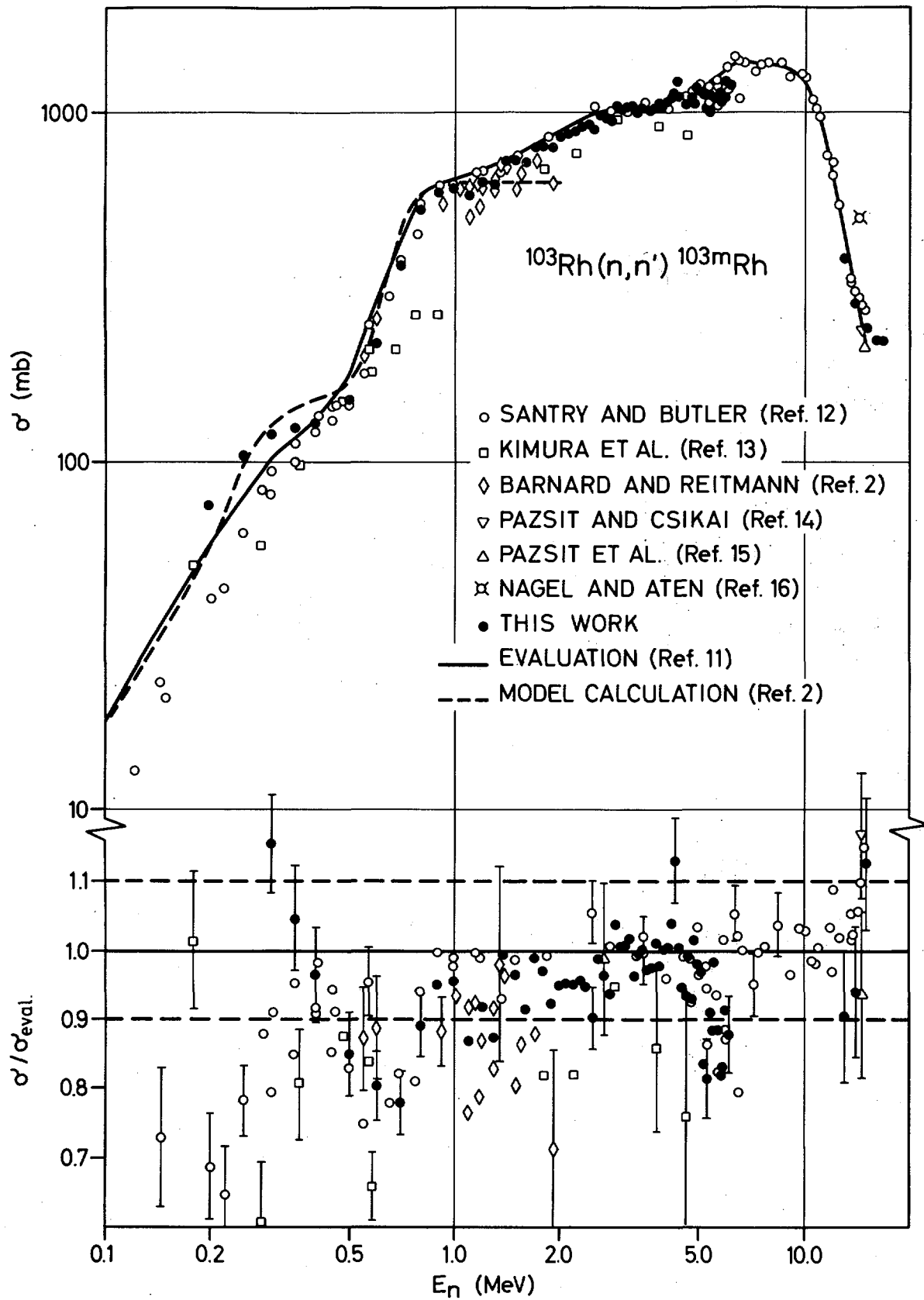


Figure 1.8 Plot of the present results together with existing data. In the lower part the same data are plotted as ratios to the UKNDL DFN94 evaluation.

Two approaches are presently examined:

- determination of the cross section via tritium produced and retained in metallic lithium samples (activation method),
- determination of the cross section via observation of tritons emitted from a thin LiF layer (direct detection method).

The differential ${}^7\text{Li}(n,t)$ cross sections are determined relative to the differential $\text{H}(n,n)$ cross sections:

$$\frac{d\sigma_{\text{Li}}}{d\Omega}(\cos \vartheta_i) = k_i \cdot \frac{\Omega_1}{\Omega_i} \cdot \frac{N_{\text{H}}}{N_{\text{Li}}} \cdot \frac{f_i C_i}{C_{\text{H}}} \cdot \frac{d\sigma_{\text{H}}}{d\Omega}(\cos \vartheta_1) \quad i = 1, 2, \dots, 5$$

The differential n-p scattering cross sections are believed to be known with $\pm 1.5\%$ accuracy. The ratios of the detector solid angles are determined with the ${}^{241}\text{Am}$ test source to an accuracy of $\pm 2.5\%$. These ratios are in good agreement with calculations based on geometry. The factors k_i take into account small corrections due to the inhomogeneous neutron irradiation of the sample foil. N_{Li} and N_{H} denote the number of ${}^7\text{Li}$ atoms in the sample foil and the number of H atoms in the radiator foil, respectively. C_i and C_{H} stand for the number of observed tritons in detector i and the number of recoil protons, respectively. Typical net triton counts observed per run were $C_i = 1000, 3000, 1000, 300, 200$ for detector 1 to 5 respectively. f_i is an important correction for the losses of low energy tritons due to the finite thickness of sample foil and ΔE -counters.

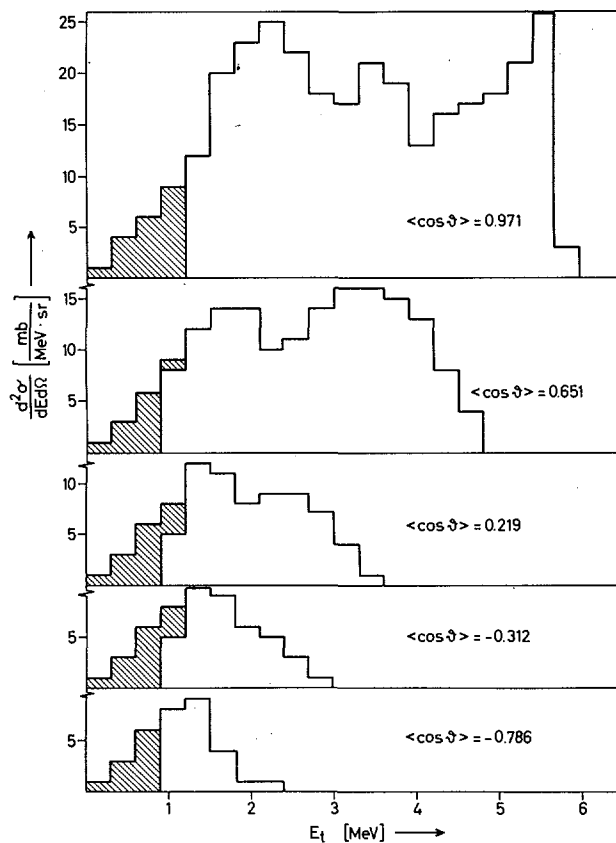


Figure 1.9 The laboratory triton energy distribution at 9 MeV neutron energy as calculated from the observed spectra taking into account the energy calibration by an ${}^{241}\text{Am}$ -source and the energy losses in the sample material and the counter gas. These spectra have been extrapolated to zero energy as indicated by the hatched areas. An uncertainty of $\pm 50\%$ has been assumed for this extrapolation.

The identification of the tritons is based on the $\Delta E-E$ diagramme. As an example the spectra of all five detectors at 9 MeV are given in Fig.1.9. Many reactions types - including three-particle break-up and two-step reactions - contribute to the triton emission, which makes spectrum interpretation difficult. These spectra have been extrapolated to zero energy. The corresponding corrections vary from 6 % at forward angle and 10 % to nearly 100 % at backward angle and 6 MeV neutron energy. We have assumed a ± 50 % uncertainty for these extrapolations and these uncertainties determine essentially also the uncertainties of the differential cross sections as given in Table 1.1.

TABLE 1.1.

Obtained differential and angle integrated cross sections of ${}^7\text{Li}(n,\alpha t)$

E_n (MeV)	DET 1		DET 2		DET 3		DET 4		DET 5		σ (mb)
	$\langle \cos \vartheta \rangle$	$\frac{d\sigma}{d\Omega} (\frac{\text{mb}}{\text{sr}})$									
6.00 \pm 0.14	0.971	97 \pm 16	0.649	53 \pm 8	0.226	20 \pm 5	-0.285	8 \pm 2	-0.775	2 \pm 1	318 \pm 60
7.00 \pm 0.11	0.971	95 \pm 7	0.651	49 \pm 3	0.229	23 \pm 4	-0.283	12 \pm 4	-0.790	3 \pm 1	330 \pm 42
7.96 \pm 0.09	0.971	108 \pm 12	0.648	60 \pm 5	0.222	29 \pm 4	-0.305	18 \pm 4	-0.777	8 \pm 2	423 \pm 54
9.00 \pm 0.08	0.971	89 \pm 7	0.651	49 \pm 4	0.219	23 \pm 2	-0.312	14 \pm 3	-0.786	10 \pm 2	352 \pm 39
9.97 \pm 0.07	0.971	95 \pm 7	0.652	54 \pm 4	0.225	24 \pm 2	-0.320	17 \pm 3	-0.787	14 \pm 3	383 \pm 41

The differential (n,t) cross sections obtained in this way are shown in Fig. 1.10 together with results obtained at Los Alamos ⁽¹⁾ using Li-loaded photoplates.

Integration over $\cos \vartheta$ was performed with five different assumptions for the angular distribution. With the assumption of a rectangular histogramme - where the widths of the $\cos \vartheta$ intervals are determined by the weighted aperture functions - the results given in Table 1.1 are obtained. The other assumptions lead to results within ± 3 % of these values.

(1) L. Rosen, L. Stewart, Report LA 2643 (1956)
and
L. Rosen, L. Stewart, Phys. Rev. 126, 1150 (1962)

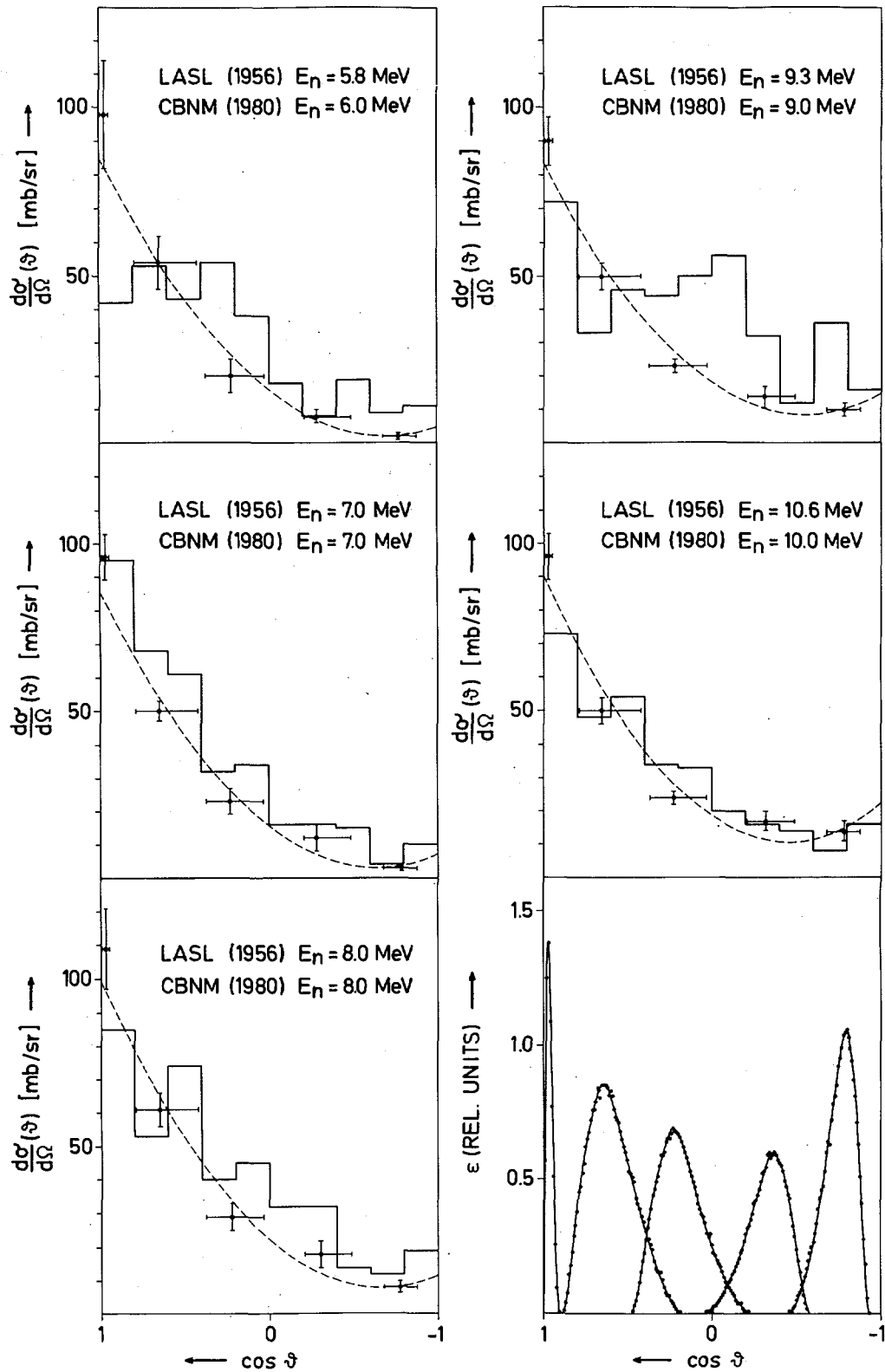


Figure 1.10 The 25 differential cross sections as obtained in this work. The dashed line is a three term Legendre polynomial fit. This fit together with the aperture functions given at the right bottom, was used to derive $\cos \theta$ values. The horizontal bars represent the FWHM of the weighted aperture functions. The shown histogrammes are results obtained in 1956 at Los Alamos using Li-loaded photo plates.

In Fig. 1.11 our results are compared with very recent results from Harwell (1), Argonne (2) and Los Alamos (3) and with ENDF/B-IV.

1.5 Various Measurements

Neutron spectra from (a,n) reactions

G. Jacobs, H. Koppelmans*,
H. Liskien

A neutron detector system based on NE 213 liquid scintillation has been set up for both time-of-flight spectrometry and proton-recoil spectrometry. The neutron time-of-flight, the proton-recoil energy and a signal depending on the shape

of the pulse (PSA) are stored, event by event, in a data acquisition and processing system ND 6660. The dynamic range of the pulse-height-spectrum is 1 : 100 with a bias setting of 30 keV electron energy. The derivation of the PSA-signal can occur using the CANBERRA 2160, the LINK 5010 and the ORTEC 552. An experimental intercomparison has been made with monoenergetic neutrons of 3 MeV energy produced via the $T(p,n)^3He$ reaction using 3.8 MeV protons. The total counting rate was about 220 cps. The results of the intercomparison are given in Fig. 1.12.

We have chosen to continue the work with the CANBERRA 2160 for the following reasons:

- the RG-values are slightly greater,
- the separation between the gamma peak and the neutron peak is better especially for small energies,

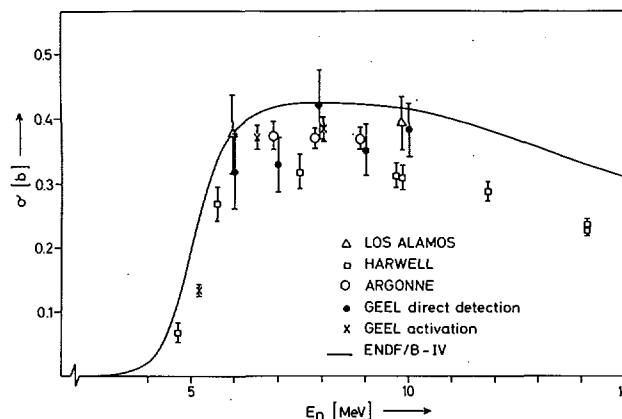


Figure 1.11 The result of this work together with other results published very recently. The two Los Alamos results are determined by detection of inelastically scattered neutrons. The points from Harwell and Argonne are obtained using the activation method. All these results were not available for the ENDF/B-IV evaluation.

(1) M.T. Swinhoe, C.A. Uttley, Proc. Int. Conf. of Nucl. Cross Sections and Technology, University of Tennessee, Knoxville, USA, October 22-26, 1979 NBS Special Publication 594, 246

(2) D.L. Smith, M.M. Bretscher, J.W. Meadows, to be published in Nuclear Science and Technology

(3) P.W. Lisowski, G.F. Auchampaugh, D.M. Drake, M. Drosy, G. Haouat, N.W. Hill, L. Nilsson, Report LA-8342 (1980)

* T.H. Eindhoven, the Netherlands

- additional electronic units are necessary to get the needed positive output signal from the LINK 5010,
- it was impossible to obtain information on the electronic circuits of the LINK 5010.

Calibration measurements have been performed in the energy region from 200 keV to 7 MeV relative to the angular distributions of the $T(p,n)^3\text{He}$ and the $D(d,n)^3\text{He}$ source reactions. At 2.0 MeV and 5.5 MeV neutron energy absolute measurements were performed using a proton-recoil telescope. The resulting absolute efficiencies are given in Fig. 1.13.

The accuracy is estimated to be 5%. In addition absolute proton-recoil distributions have been determined at 21 monoenergetic neutron energies between 0.2 and 7.0 MeV (see Fig. 1.14).

These distributions are used in the unfolding code FORIST to obtain neutron spectra via proton-recoil spectra.

As an example for application the energy spectrum of neutrons emitted at 0° while bombarding

a thick aluminium target with 4.5 MeV α -particle is shown in Fig. 1.15.

^{10}B Mass determination by (n,α) reaction rates

R. Buyl, E. Wattecamps

Natural boron deposits (B 184 and B 187) were made by evaporation. At the BR-1 reactor, SCK-CEN, Mol, the amount of ^{10}B on the samples, relative to a reference sample B 74, was measured by neutron irradiation. The support,

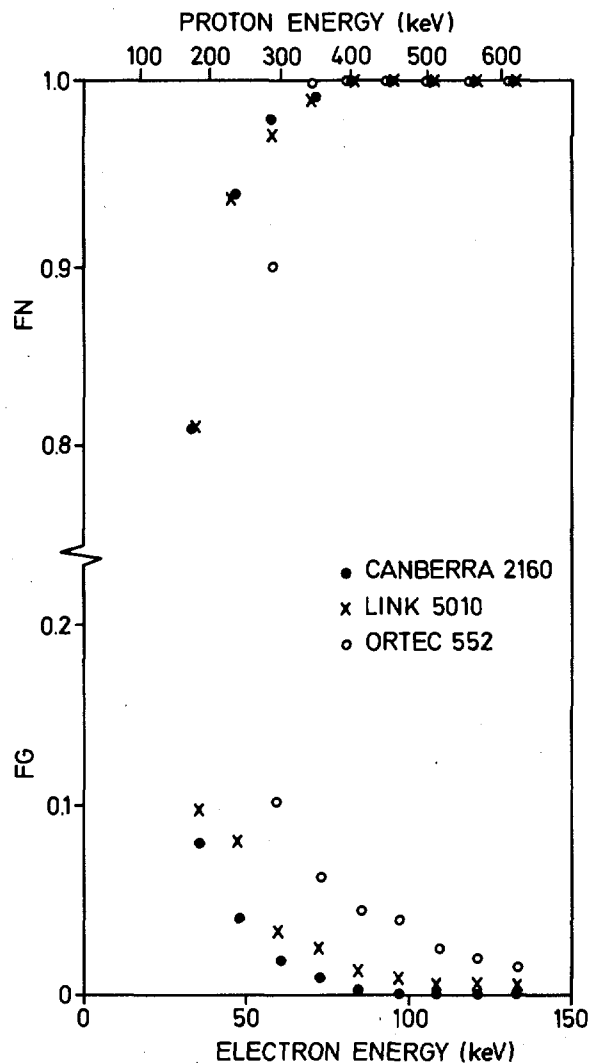


Figure 1.12 The fraction of neutrons (FN) and the fraction of gammas (FG) registered in the neutron region is given as function of the proton and electron energy, respectively.

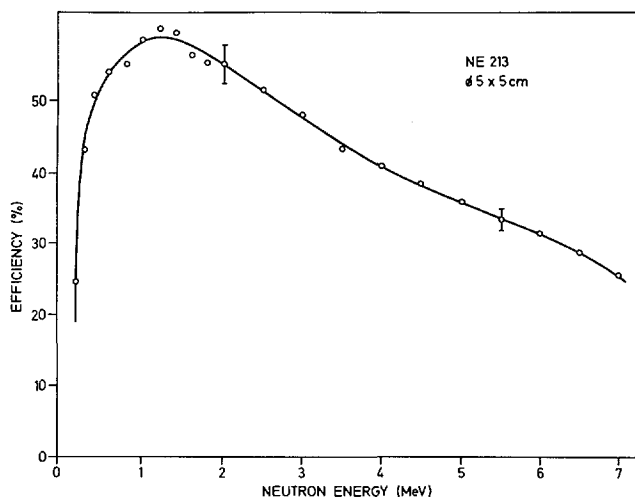


Figure 1.13 The measured absolute efficiencies for the NE 213 liquid scintillation as function of the neutron energy.

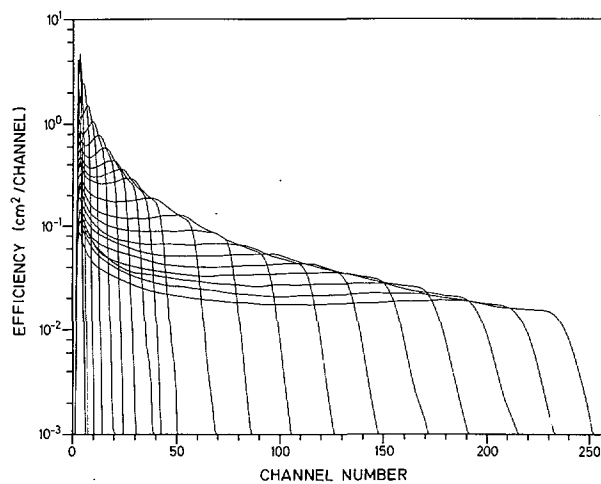


Figure 1.14 The 21 measured absolute proton-recoil distributions at neutron energies between 200 keV and 7 MeV.

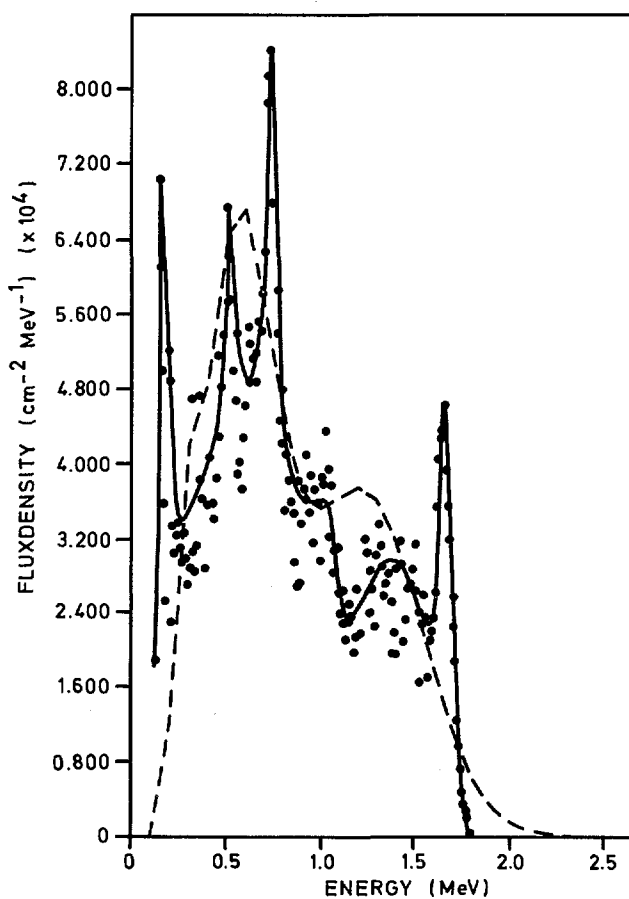


Figure 1.15 The energy spectrum of neutrons emitted in the direction of the incident α -particle beam from the $\text{Al}(\alpha, n)$ reaction. The determination used the proton-recoil method (---) and the time-of-flight method (—).

the size and the backing of the samples B 184 and B 187 are identical with existing reference samples. The new samples were put in the sample changer device together with reference samples B 74 and B 73. See reference (1). The reference samples are known by very careful weighing and analytical measurements to have a total ^{10}B mass of $98.536 \mu\text{g} \pm 0.55 \%$ and $77.922 \mu\text{g} \pm 0.55 \%$ respectively. See also reference (2). The $^{10}\text{B}(n,\alpha)^7\text{Li}$ reaction rates observed in a collimated neutron beam at the BR-1 reactor running at 600 kW are given in Table 1.2 together with the ^{10}B mass deduced from these measurements.

TABLE 1.2.

Sample number	(n, α)rate	monitor	time in sec.	^{10}B in μg	Relative error
B 73	467.010	10^5	375,6		
B 184	44.682	10^5	375,5	7,463	$\pm 0,86 \%$
B 74	589.932	10^5	375,8		
B 187	90.687	10^5	376,8	15,145	$\pm 0,79 \%$

The error on the mass of ^{10}B on the entire sample is deduced from the square root of the sum of the squares of errors on monitor counts, sample counts and mass of reference samples. The systematic error due to inequal positioning of the samples is negligible. The positioning of all the samples is identical within 0.01 mm. Proper positioning is confirmed by the measured (n, α) rate ratio of B 74 to B 73, namely: $1.263 \pm 0.35 \%$; which corresponds well with the ratio of their weights $1.264 \pm 0.78 \%$.

The total errors so far obtained are 0.86 % and 0.79 % respectively, but these could be reduced by increasing the count rate of the monitor and by increasing the time of irradiation. The limitation of accuracy for the moment is the error of 0.55 % on the mass determination of the reference samples. For samples of geometrical size different from the reference samples the lower error limit is larger.

(1) A.J. Deruytter, J. Spaepen, P. Pelfer, Journal of Nucl. Energy, Vol. 27, p. 645 (1973)

(2) H.L. Eschbach, Nucl. Instr. and Meth. Vol. 102, p. 469 (1972)

Neutron induced charged particle reactions on ^{40}K

M. Ashgar[★], R. Barthélémy, A. Emsallem^{★★}, C. Wagemans, H. Weigmann

The $^{40}\text{K}(n,p)^{40}\text{Ar}$ and $^{40}\text{K}(n,\alpha)^{37}\text{Cl}$ reactions were measured with thermal neutrons at ILL, Grenoble, and with neutrons in the energy range from 0.02 eV to 70 keV at GELINA. Fig. 1.16 shows the measured sum of the (n,p) and (n, α) cross sections in the keV neutron energy range. The proton and alpha-particles were detected with a large surface barrier detect, and the neutron energy was measured by time-of-flight.

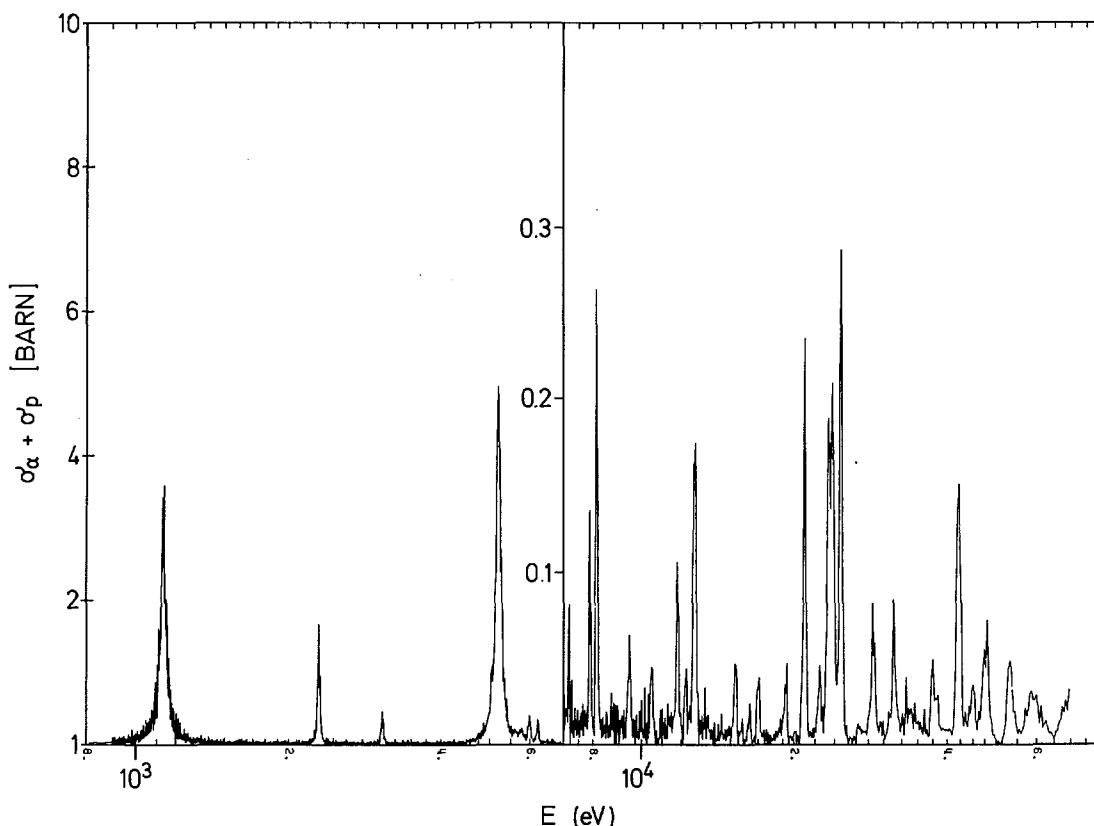


Figure 1.16 The $^{40}\text{K}(n,\alpha)$ and $^{40}\text{K}(n,p)$ reaction cross section between 0.8 and 70 keV neutron energy.

The observed resonances are due to s-wave (compound spin $J = 7/2^-$ or $9/2^-$) or p-wave ($J = 5/2^+$ to $11/2^+$) neutron interaction. They are listed in Table 1.3 together with some information on their parameters, obtained from a resonance area-analysis. The strong fluctuations in the relative p- and α -yields can be understood in terms of the involved angular momenta; they also give the argument for the few spin and parity assignments in Table 1.3.

★ ILL-Grenoble, France
 ★★ IPN-Lyon, France

TABLE 1.3.

Observed resonances for neutron interaction with ^{40}K

E_r (keV)	$g_n^{\Gamma} \Gamma_p / \Gamma$ (MeV)	$g_n^{\Gamma} \Gamma_{a_0} / \Gamma$ (MeV)	J^{π}
1.128	< 0.3	43 + 4	9/2 ⁻
2.291	< 0.6	28 + 2.5	
3.060	13 + 1.5	1 + 0.25	$\pi = +$
5.038	< 3	1100 + 90 [*])	9/2 ⁻
5.177			
5.60			
5.73			
5.98	31 + 3.5	11 + 5	
6.21	3.5 + 1	39 + 5	
(6.6)	5 + 2	< 2 ⁻	
7.15	< 0.5	7.5 + 1.5	
7.87	1 + 0.5	16 + 2.5	
8.10	< 1 ⁻	34 + 4	
9.42	9 + 1.5	6 + 1.5	($\pi = +$)
10.4	10 + 2.5	9 + 2.5	($\pi = +$)
11.7	15 + 1.5	38 + 6	($\pi = +$)
12.2	< 1 ⁻	12 + 2	
12.7	< 5	112 + 12	
15.3	7 + 2.5	30 + 5	($\pi = +$)
(15.7)			
16.3	< 5	10 + 3	
17.0	< 2	32 + 6	
19.3	< 3	32 + 6	
20.9	17 + 5	270 + 30	7/2 ⁽⁺⁾ 9/2 ⁺
22.4			
23.3			
23.7			
24.6			
(26.6)			
28.4			
(29.5)			
31.3			
37.4			
42.0			
44.9			
47.9			
53.2			
58.5			
(69)			

*) at least 80 % of this strength is in the 5.177 keV resonance.

The thermal cross sections have been obtained as $\sigma_{np} = (4.4 \pm 0.9)b$ and $\sigma_{na} = (0.39 \pm 0.08)b$. None of the observed resonances can explain the σ_{np} value, and it is therefore assumed that the thermal cross-sections are dominated by a $7/2^-$ bound state. The density of the observed resonances can be compared to the density of spin 1/2 compound states observed as resonances in the reaction $^{40}\text{Ar} + p$ by Keyworth et al. (1). This comparison allows a direct determination of the spin cut-off parameter of the level density. A value of $\sigma^2 = 16.0 \pm 4.4 - 3.4$ is obtained.

Investigation of the neutron capture mechanism in ^{88}Sr

B.J. Allen^{*}, R. Shelley, G. Vanpraet^{**}, T. van der Veen

The asymmetric capture resonances observed in ^{54}Fe have been interpreted to be a manifestation of valence neutron capture mechanism in the 3s strength function region at the $N = 28$ closed neutron shell. A similar effect is expected when the 3p single particle state becomes unbound at the $N = 50$ magic neutron number.

Earlier capture measurements at ORELA⁽²⁾ showed a strong correlation between the p-wave reduced neutron widths and the corresponding radiation widths. It is therefore expected that interference effects may also be observed in the capture channels for the strong p-wave resonances near 300 keV and 550 keV. A $\text{Sr}(\text{NO}_3)_2$ -sample, highly enriched in ^{88}Sr , was made available on loan from ORNL via the AAEC. The resonance capture yield has been measured from 0.2 to 600 keV using C_6D_6 detectors at a 60 m station of GELINA. The yields in the vicinity of 300 keV appear to be asymmetric for the strong p-wave resonances. However statistics are inadequate above 500 keV. High bias data were also recorded in an endeavour to obtain the ground state partial capture cross-section. This would permit a more direct comparison with the valence model. A moderated neutron target was used for the present measurement. An unmoderated target would give a much higher neutron flux above 500 keV but may result in severe γ -flash problems. This latter option is under investigation.

(1) G.A. Keyworth, G.C. Kijker Jr., E.G. Bilpack, H.W. Newson, Nucl. Phys. 89, 590 (1966)

(2) J.W. Boldeman, B.J. Allen, A.R. de L. Musgrove, R.L. Macklin, R.R. Winters, Nucl. Phys. A269, 397 (1976)

^{*} Visiting scientist from AAEC Lucas Height
^{**} Rijksuniversitair Centrum, Antwerpen, Belgium

Studies on the thick target $^9\text{Be}(d,n)^{10}\text{B}$ neutron source

A. Crametz, H.-H. Knitter, D.L. Smith^{*}

It is not generally realized that the neutron source reactions $^7\text{Li}(d,n)^8\text{Be}$ $Q = 15.03$ MeV and $^9\text{Be}(d,n)^{10}\text{B}$ $Q = 4.36$ MeV are very productive at even rather modest incident deuteron energies, when the deuterons are stopped completely in the target material. Since our Van de Graaff will be equipped with a sub-nanosecond pulsing system, this white neutron source can be favourably compared in the MeV range with other powerful sources such as the electron linacs, LAMPF or tandem accelerators using the same source reactions.

To study the possibilities for neutron experiments, the determination of the spectral shape and the absolute neutron yield at zero degree with respect to the incident beam for the $^9\text{Be}(d,n)^{10}\text{B}$ reaction at 7 MeV deuteron energy is being made. In order to compare and to proof the powerfulness of this source with respect to others, the total cross section of carbon, ^{28}Si and ^{232}Th will be measured in the energy range from 400 keV to 10 MeV.

High Resolution Total Cross Section Measurements

C.R. Jungmann^{***}, E. Cornelis^{****}, L. Mewissen^{**}, F. Poortmans^{**}

A 400 m neutron flight path has been equipped for high resolution total cross section measurements, using unmoderated neutrons for the U-target of the Linac. A typical figure for the achieved energy resolution is 340 eV (FWHM) at 1 MeV neutron energy.

As a test, the total cross section of a natural C sample has been measured between 0.5 MeV and 19 MeV neutron energy. Excellent agreement has been obtained with the data of ENDF/B-IV.

The total cross section of natural S has been measured in the energy range from 0.18 to 10 MeV. A resonance parameter analysis is presently in progress for neutron energies below 2 MeV. For most of this energy range, a multi-level-Breit-Wigner analysis code is used; where resonance-resonance interference is particularly strong, a full R-matrix code is applied.

Differential Elastic Scattering Cross Sections of Sulphur

C.R. Jungmann^{***}, E. Cornelis^{****}, L. Mewissen^{**}, F. Poortmans^{**}

An equipment to measure differential elastic scattering cross section with high neutron energy resolution has been set up at a 100 m neutron flight

^{*} Visiting scientist from ANL
^{**} SCK-CEN, Mol, Belgium
^{***} Bursary of the European Community
^{****} Rijksuniversitair Centrum, Antwerpen, Belgium

path of GELINA. It consists of six plastic scintillator (NE 110) detectors mounted around a sample which is placed in a vacuum chamber. Experiments were completed for sulfur in the energy range from 100 keV up to 2 MeV. Data have been taken for 11 angles between 26° and 154° (lab. angle). The data analysis has been started. The equipment has now been installed at the 400 meter flight-path and an additional run on sulfur has been started. The experiment will cover the energy range from 300 keV up to the inelastic threshold at 2.23 MeV.

1.6 Standard Neutron Data

Angular distributions of the ${}^6\text{Li}(n,t){}^4\text{He}$ reaction

H.-H. Knitter, C. Budtz-Jørgensen, D.L. Smith^{*}, H. Bax, R. Vogt

The ${}^6\text{Li}(n,t){}^4\text{He}$ reaction is extensively used as a standard in neutron cross section measurements, for flux normalization and in neutron spectroscopy. The high Q-value of 4.784 MeV and the smooth behaviour of its cross section below 100 keV make this reaction a nearly ideal standard. In recent years it has been discovered that the ${}^6\text{Li}(n,t){}^4\text{He}$ reaction has large angular anisotropies even down to a few keV, which, when not taken properly into account, can lead to large errors in many flux measurements. So far anisotropy data below 100 keV have only been taken at 24 and 2 keV using filtered reactor beams. It was decided to measure the ${}^6\text{Li}(n,t){}^4\text{He}$ angular distributions with the angle sensitive ionization chamber developed at JRC-Geel. This chamber was originally designed for fission fragment angular distribution work as described in the previous progress report. For the present application a double chamber loaded with two samples of $(245 \pm 2) \mu\text{g}/\text{cm}^2$ ${}^6\text{LiF}$ was constructed such that a 4π solid angle can be covered. The diameter of the deposit is 4.5 cm. Argon + 5 % CO_2 at 3.8 bar is used as counter gas. The distances d between the cathode and the Frisch grids are 25 mm and the distances between the grids and their corresponding anodes are 6 mm. Under these conditions tritons produced in the (n,t) reaction will be stopped in the space between cathode and grids for neutron energies up to 0.5 MeV. The information on the triton angle with respect to the direction of the neutron beam is contained in the pulse height of the cathode signals ($q_{\text{ca}} = E(1 - \frac{\bar{x}}{d} \cos \Theta)$), where \bar{x} is the distance from the origin of the particle track to the centre of the ion distribution. The energy is taken from the anode signals $q_{\text{an}} = E$. The chamber was mounted at

* Visiting scientist from ANL

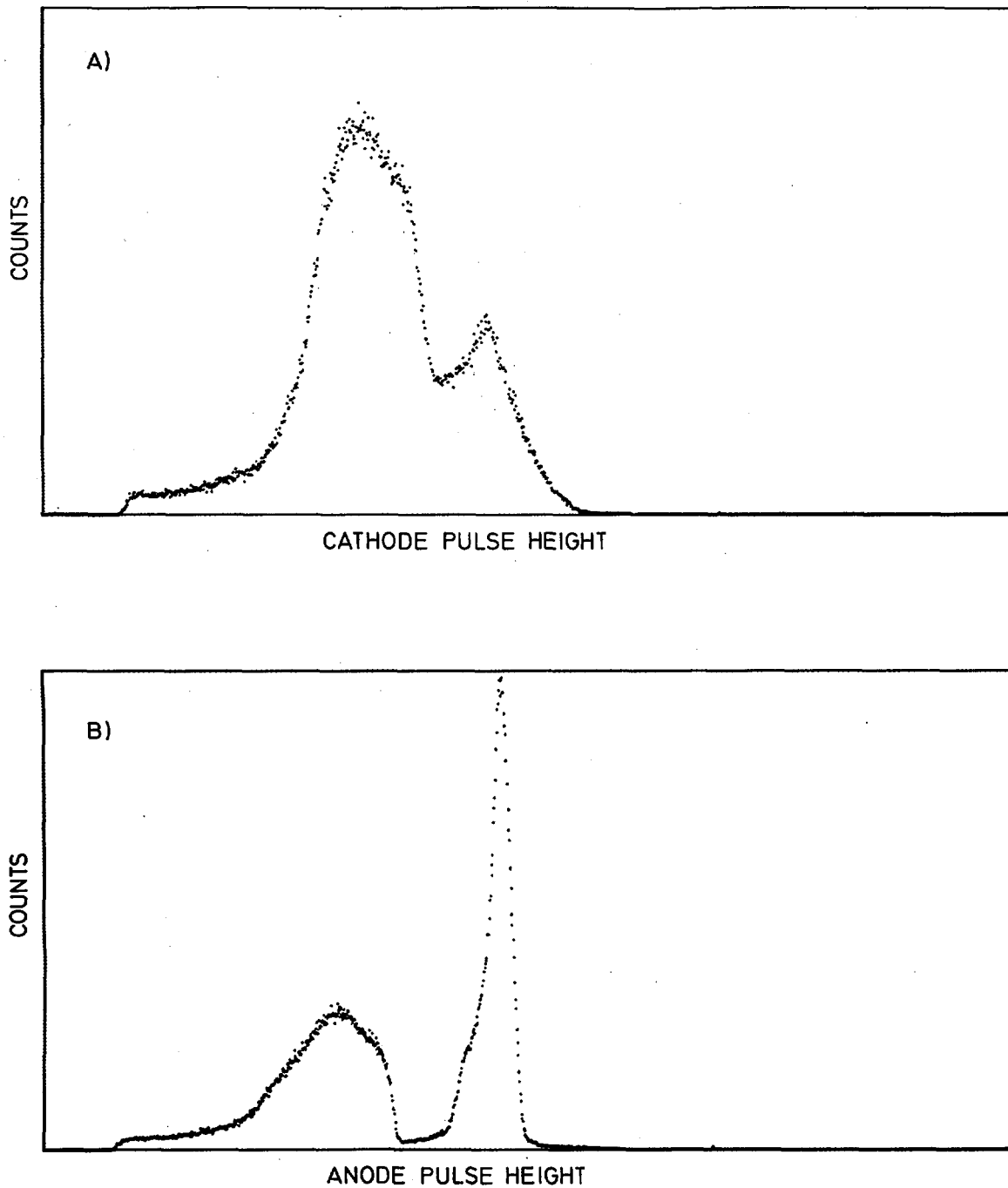


Figure 1.17 A) shows the triton and alpha particle pulse height spectrum following the ${}^6\text{Li}(n,t){}^4\text{He}$ reaction, as obtained from the cathode signals. The spectrum covers all particles emitted in the whole solid angle from 90° to 180° with respect to the incident neutron beam and produced by neutrons having energies between 100 eV and 0.5 MeV.

B) same as A) but obtained from the anode. The energy spectrum shows a good separation between triton and alpha particles.

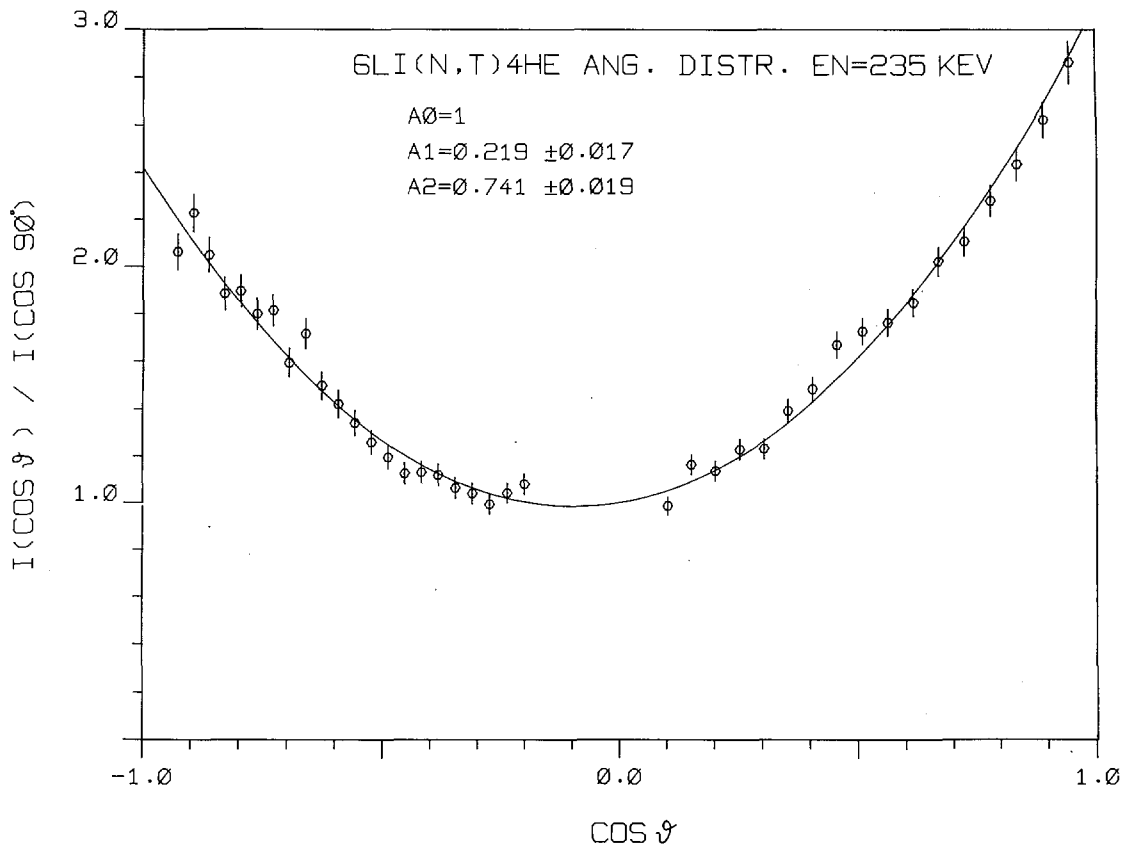
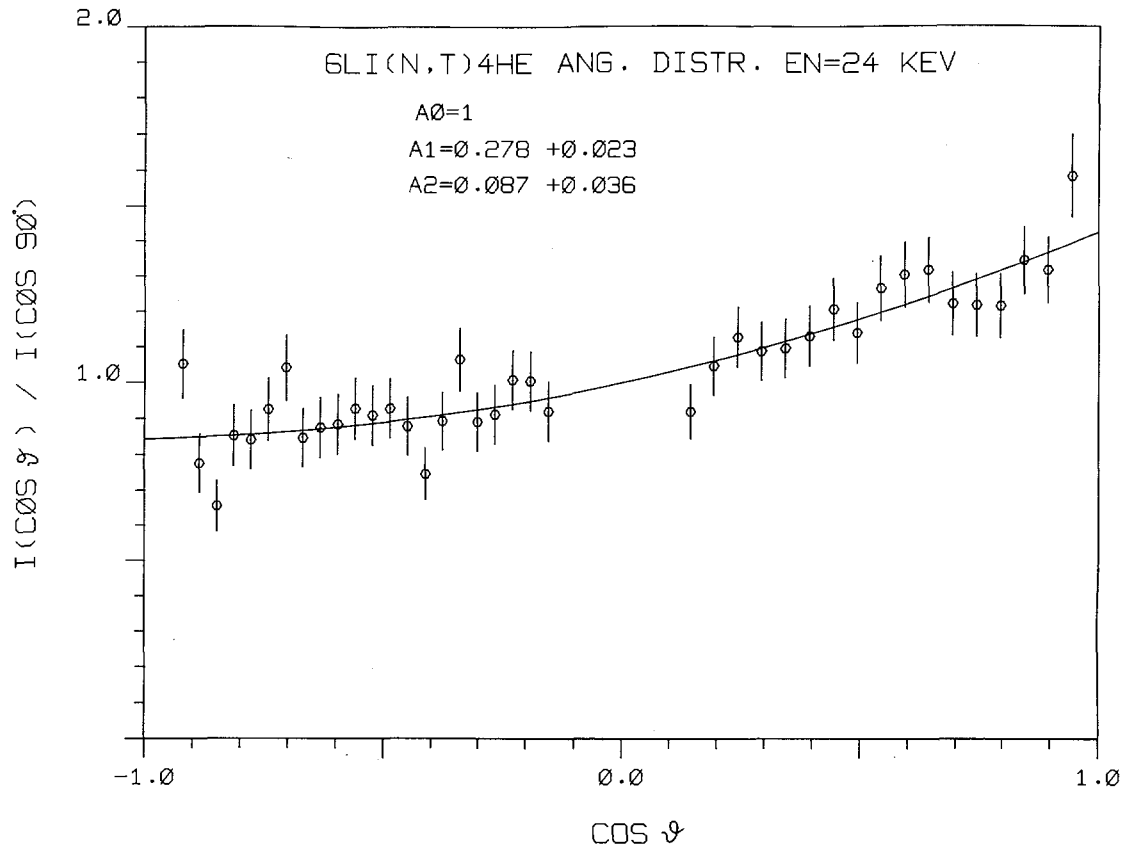


Figure 1.18 Two C.M.-angular distributions of the tritons produced in the ${}^6\text{Li}(n,t){}^4\text{He}$ reaction at 24 keV and 235 keV respectively. The full line represents least square fits with Legendre polynomials up to second order.

30 m from the neutron producing target of the Linac. The neutron time-of-flight information is obtained from the cathode signals feeding them to a constant fraction discriminator and a 10 ns time coder. The pulse heights are, together with the digitized output from the time coder, stored event by event on magnetic tape. The angular distributions of the ${}^6\text{Li}(n,t){}^4\text{He}$ reaction are, with present set-up, investigated in a neutron energy range between 10 eV and 0.5 MeV. Above that energy the information is disturbed by pulses induced by the Linac γ -flash and by the fact that the triton range becomes longer than the distance between grid and cathode.

Fig. 1.17 shows typical pulse height spectra of the cathode and anode signals integrated over a neutron energy range from 100 eV to 0.5 MeV. The energy spectrum from the anode demonstrates a clear separation between alpha and triton particles.

Fig. 1.18 shows preliminary C.M.-angular distributions obtained at 24 keV and 235 keV respectively.

It should be stressed that the great advantage of this detector is that up to 40 angular points are measured simultaneously.

A preliminary evaluation in the whole neutron energy range of the ratio of the tritons emitted in the forward and the backward hemisphere in the laboratory system was carried out. The result is shown in Fig. 1.19.

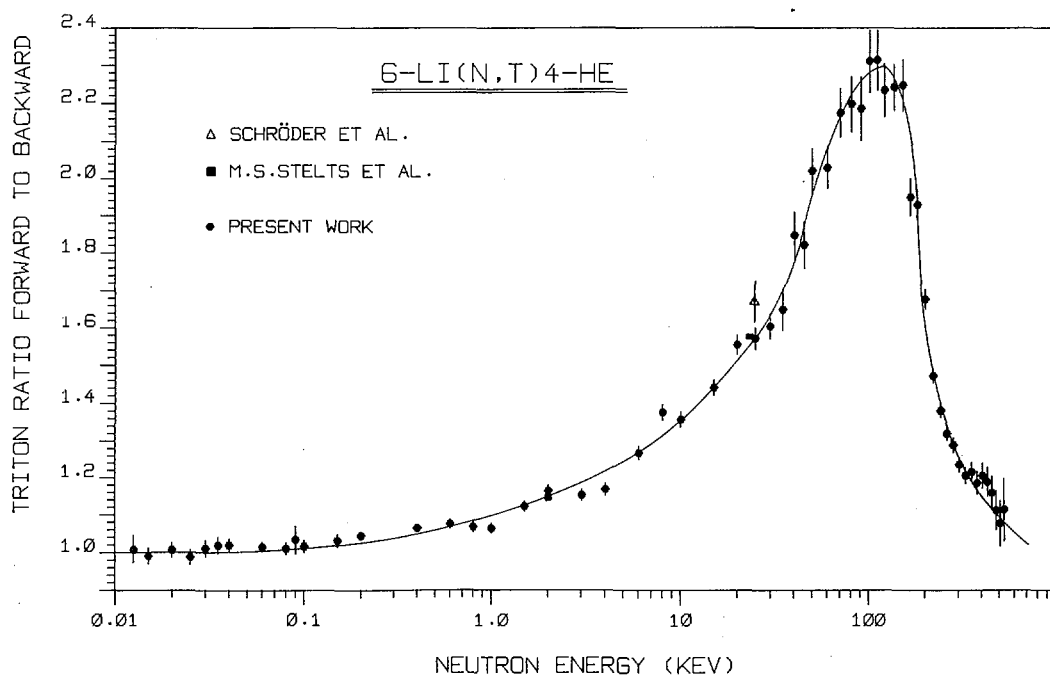


Figure 1.19 Preliminary ratio of tritons of the ${}^6\text{Li}(n,t){}^4\text{He}$ reaction emitted in the forward and backward hemisphere in the laboratory reference system with respect to the neutron beam direction. The symbols Δ , \blacksquare , \bullet represent results of measurements of Schröder et al., Stelts et al. and of the present work.

This figure shows that already at a neutron energy as low as 100 eV a deviation from symmetry becomes visible. Comparison is also made with the two recent data points of Stelts and Chrien ⁽¹⁾ and Schröder et al. ⁽²⁾, who have measured with the filtered reactor beam technique at 2 keV and 24 keV incident neutron energy. The evaluation of the angular distributions is being done and the corresponding Legendre polynomial coefficients were obtained. The measurements will be continued towards higher neutron energies at the Van de Graaff accelerator. It is hoped that the measurements at higher energies can help to determine the part of the reaction which may proceed via the direct deuteron exchange process.

1.7 Evaluation and Underlying Physics

Effect of parameter fluctuations on the average fission cross section in the presence of intermediate structure

H. Weigmann

It has been shown by Lynn and Back ⁽³⁾ that the presence of intermediate structure can significantly reduce the average fission cross section in the threshold and sub-threshold region as compared to the one calculated from the same average parameters in the absence of intermediate structure. However, the equations given in ref. ⁽³⁾ are obtained in a picket-fence model approximation for both, class I- and class II states; the influence of statistical fluctuations of the class I and class II level parameters is separately and essentially qualitatively discussed.

In order to get a more quantitative insight into the combined effect of the statistical fluctuations of class I and class II level parameters, a series of numerical cross section calculations from Monte-Carlo simulations of level sequences has been performed for a few sets of typical average parameters. First, a sequence of class II levels with average spacing $D_{II} = 500$ eV is generated and their fission (Γ^{\uparrow}) and coupling (Γ^{\downarrow}) widths are independently sampled from Porter-Thomas distributions (valid for sub-barrier energies). Then, a sequence of class I levels with average spacing $D_I = 10$ eV is generated; their neutron widths are sampled from a Porter-Thomas distribution

(1) M.L. Stelts et al., Phys. Rev. C, 19, 1159 (1979)

(2) I.G. Schröder et al., Proc. Int. Conf. of Nucl. Cross Sections and Technology, Washington D.C. (1975), NBS Spec. Publ. 425, 240

(3) J.E. Lynn, B.B. Back, J. Phys. A7, 395 (1974)

with average value $D_I/2\pi \times T_n$; and a constant capture width $\Gamma_C = D_I/2\pi \times T_C$ is assumed. For each class II level, depending on whether $\Gamma_{\downarrow} + \Gamma_{\uparrow}$ is smaller or larger than $0.5 D_I$, it is decided whether its coupling to the class I resonances is treated in perturbation theory or whether a Lorentzian energy dependence of the fine structure fission widths is assumed. In the latter case, the Lorentzian profile defines the expectation value of the fine structure fission widths and individual values are sampled from Porter-Thomas distributions with this energy-dependent expectation value. In the perturbation case the class II coupling width defines an average squared coupling matrix element and individual values are sampled from a Porter-Thomas distribution with this average.

From the sequence of resonances constructed this way the average cross section for a given compound nuclear spin is calculated and the procedure repeated a sufficient number of times to obtain a reasonably accurate average. The whole calculation has been done for a number of combinations of barrier transmission coefficients T_A and T_B , and the results plotted in Fig. 1.20 as a function of the fission probability P_F (1). In fact, different combinations of T_A and T_B corresponding to the same P_F yielded very similar results as long T_A and T_B are smaller than 0.5, i.e. one is dealing with a subbarrier case (above the lower barrier the assumption made in these model calculations, e.g. Porter-Thomas distributions for the class II widths, would be invalid anyhow).

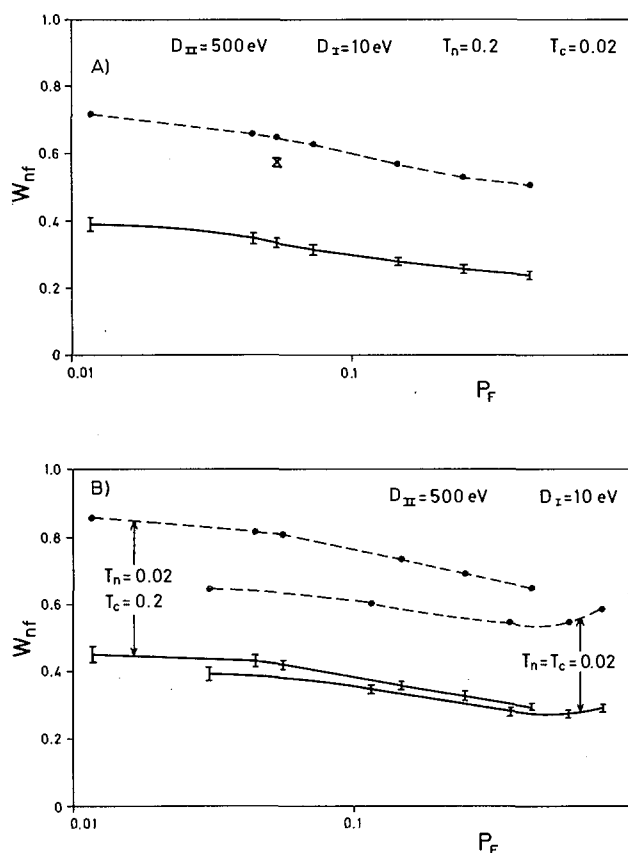


Figure 1.20 A) Reduction of fission cross section due to statistical fluctuation of level parameters in a case with intermediate structure — results of Monte Carlo simulation --- usual fluctuation correction for purely statistical fluctuations B) Same as A) for two further sets of average parameters.

(1) J.E. Lynn, B.B. Back, J. Phys. A7, 395 (1974)

The full curve of Fig. 1.20 represents the ratio

$$W_{nf} = \frac{\sigma_{nf} \text{ (simulation)}}{\sigma_{nf} \text{ (stat.model without fluct.corr.)}}$$

of the fission cross section obtained from the Monte-Carlo simulation and the one calculated from the fission probability P_F of ref. (1) without any fluctuation correction. For comparison, the broken line gives the width fluctuation factor calculated by the usual prescription (2) which, however, is not valid in a situation with intermediate structure.

The fixed parameters of Fig. 1.20 A) (D_{II} , D_I , T_C) were chosen such as to be characteristic of an even-even actinide target nucleus.

The T_n of Fig. 1.20 B) may correspond to s-wave neutrons at about 100 keV neutron energy. Similar results for two other choices are shown in Fig. 1.20 B); the large T_C for one of these choices may be thought of as crudely representing a larger number of inelastic neutron channels the fluctuations of which roughly cancel.

The common feature of all three parameter combinations in Fig. 1.20 is that the actual suppression of the fission cross section due to statistical fluctuations of level parameters as obtained from the Monte-Carlo simulation, is much larger than the one which would be calculated from the usual fluctuation correction factor.

Application of the level density systematics

G. Rohr

A contribution has been made to the International Conference on Nuclear Physics, Berkeley, August 1980, with the title: "Pairing Energies and Single Particle State Densities Studied by means of the Level Density Systematics". The contribution included the following:

A method to study residual interactions in nuclei was worked out. It is based on energy levels of excited nuclei observed at energies where the number of states is large enough to determine the level density and where the excitation energy is large compared to the depression of the groundstates caused by the pairing energy, the most important short range force. Both conditions are fulfilled for the neutron resonances observed at neutron separation energy. A level density systematics is performed based on the

(1) J.E. Lynn, B.B. Back, J. Phys. A7, 395 (1974)

(2) L. Dresner, Report ONRL 2659 (1959)

level density of compound resonances (newly evaluated ⁽¹⁾). It is interpreted by comparison to calculated values of the level density of doorwaystates resulting from the first step of the compound process ⁽²⁾.

The deviation of the level density parameter 'a' from a linear dependence on the atomic number A indicates two types of structures (Fig. 1.21).

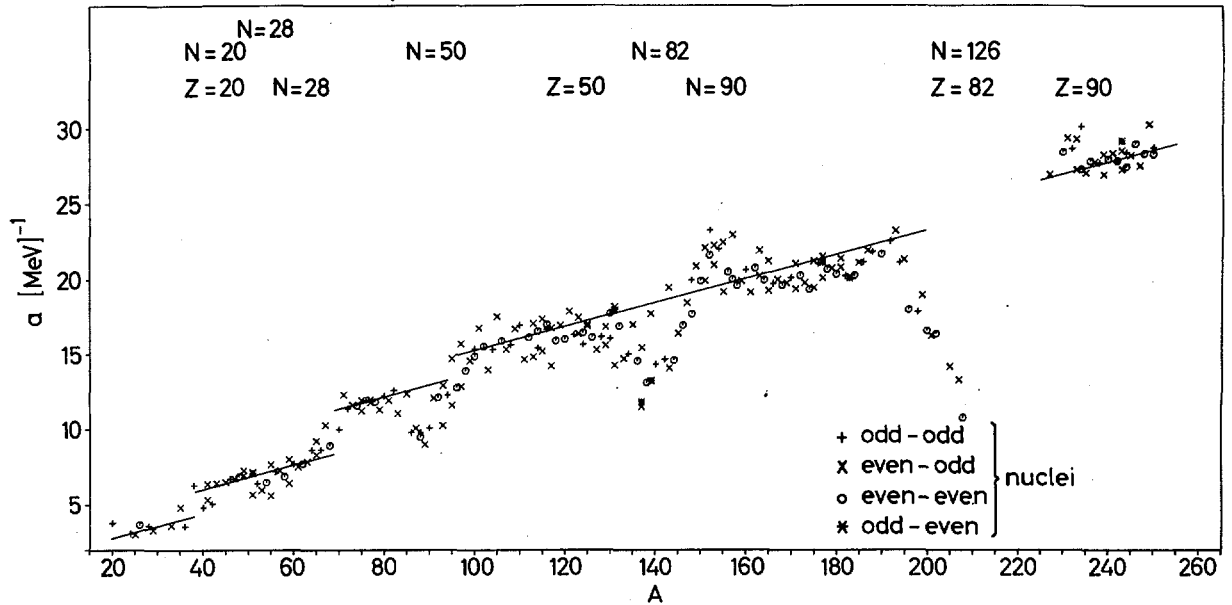


Figure 1.21 Level density systematics.

First there are the usual shell effects with "dips (20, 28, 50, 82, 126) and bumps (90)" at specific N and Z values reflecting changes of the level density of single particle states at the Fermi surface energy. Second there are distinct steps (three in total) of the level density parameter 'a' at certain A values which we interpret as evidence for a successively more important contribution from higher hierarchies of states in the compound nucleus formations.

The lines in between successive structures seen in the Fig. 1.21 are defined by using odd-odd compound nuclei, where pairing corrections are minimised. Based on this interpretation of the level density systematics the pairing energy Δ and shell energy S are determined and possibilities of adjusting Nilsson single particle states are discussed. Using $(\Delta + S)$ together with the liquid drop model a "semi-empirical binding energy formula" can be obtained. It is hoped with this and the level density systematics to provide insight into the effects of short range forces.

(1) G. Rohr, L. Maisano, R. Shelley, to be published

(2) G. Rohr, R. Shelley, Int. Conf. on Neutron Physics and Nuclear Data for Reactors and other Applied Purposes, Harwell 1978, p. 478

1.8 Major Research Equipment

GELINA (Geel Electron Linear Accelerator)

J.M. Salomé, R. Cools, R. Forni, F. Massardier, F. Menu, K. Meynants, P. Siméone, F. Van Reeth, C. Waller, J. Waelbers

During the covered period (01.11.1979 - 31.10.1980) the accelerator was operated as shown in Table 1.4.

TABLE 1.4.

Electron Beam Parameters of Linac

Pulse length ns	Rep. rate Hz	Peak current A	Mean energy MeV	time hours	% of the time
4 - 5	800	10	110	3141	75.7
14	800	8	100	575	13.8
14 - 20	100	8.5 - 6	100	203	4.9
2000	100	0.21	90	28	0.7
1800	250-300	0.14	44	203	4.9

On the average 6.7 neutron beams were used simultaneously for measurements. Low energy electron beams were produced eleven times for activation analysis with mean current of about 55 μ A.

The rotary uranium target was used during 575 h and successively the natural and enriched U stationary targets during 3372 h.

Autoradiographies of the stationary target have been done with a γ -camera installed along a flight path normal to the electron beam. It was observed that the beam path within the target was longer than expected which was interpreted as a crack or hole in the middle of the uranium cylinder. Therefore this target, which has been used during about 8000 beam hours, was put out of duty.

Modification of the electron injection and the prebunching cavity were designed and ordered to the firm CGR-MeV. This cavity will be adequately positioned and driven by up to 30 kW peak power. The shape of the magnetic field will be modified to get a more efficient focusing at the input of the first section. These modifications will increase the efficiency of the first section yielding a higher peak current. Also the energy spectra of the microbunches will be of better quality which is very important in view of the operation of a compression magnet to be installed in the target room. This magnet is ordered and will be delivered and installed within 14 months. Its weight is 35 tons with a pole diameter of 2.4 m. A pulse compression factor of at least 3.3 is expected, which corresponds to 3-4 ns, 40-30 A electron beams at the target starting from a beam of 12 ns, 10 A at the input of the magnet. The compression effect is due to the different paths followed in the magnetic field by the electrons with different energies. The energies in the Linac pulse decrease from the beginning to the end of the pulse.

These very much improved parameters should be available during summer 1982.

Van de Graaff Accelerators

A. Crametz, P. Falque, J. Leonard, R. Smets

During 1980, the accelerators were operational during 2990 hours (2190 hours for the CN-7 MV accelerator and 310 hours for the KN-3.7 MV accelerator). The 500 remaining hours, were used for conditioning, starting procedures and repairs.

The mechanical realisation for the first step of automatic control of the parameters of the accelerator, by using step motor driven selsyns and a data logger, is nearly completed and tests are foreseen for next year. Better time resolution for time-of-flight experiments with light ions can be achieved by a pulse compression system. The realisation, is planned in collaboration with the Max Planck Institut für Kernphysik of Heidelberg, where the relevant know-how exists. A resonator wound as a spiral in a cylindrical tank of 35 cm diameter and 20 cm length will be used. At the end of the spiral, a drift tube is attached which is aligned between two ground tubes in the tank walls on the beam axis. The resonator is powered by a commercial 20 kW radio transmitter at 105 MHz in continuous wave mode. The major part of the necessary equipment has been ordered.

Data Processing Equipment

The work load of the CBNM central computer system (IBM 370/138) has steadily been increasing over the last years, in particular for data analysis in time sharing mode.

The number of local display terminals in the IBM 3270 Information Display System has been increased from 6 to 11.

The disk storage capacity has been extended from 420 M bytes to 700 M bytes. The system programmes VS APL and VS TSI0 have been installed to improve the efficiency of interactive work on the system.

Detailed plans have been made to extend the present computer system by an IBM 4341 processor which offers four times the memory capacity and four times the interval execution speed of the present IBM 370/138 processor.

The new processor will be operated in parallel with the existing one on the basis of shared disk storage systems. Nearly all input/output units will be attached to the 4341 processor as main system assisted by the old 370/138 processor for batch processing work. The installation of the 4341 system is planned for the beginning of 1982.

Development and Test of Hardware and Software Tools for measuring Linac Neutron Spectra with a Proportional Counter

T. Babeliowsky, R. Buyl, J. Van Gils, E. Wattecamps

A methane filled proportional counter (1200 mm pressure) was used to investigate the fast neutron spectrum from 80 keV to 2 MeV of a collimated neutron beam of GELINA. The counter was built and previously used for flux measurements of monoenergetic neutron sources at the Van de Graaff accelerator ⁽¹⁾. The neutron source at GELINA was the rotating uranium target with two Be-canned water moderators. A shadow cone in the target room and a second shadow cone in the bunker wall shielded the detector from the gamma rays of the rotating uranium target. The collimation was made to get neutrons from the entire moderator. The cylindrical proportional counter of 188 mm active length and 49.8 mm active diameter was put at 198.042 m flight path distance. Its central anode wire was collinear with the centre line of the collimated neutron beam. A polyethylene collimator of 20 cm length is located in front of the counter at 196 m. This collimator has an inner diameter of 30 mm, and, in addition, a central shadow cylinder of 14 mm diameter and 20 cm length. The coaxial location of the counter and the peculiar shape and size

(1) H. Liskien, A. Paulsen, Nucl. Instr. and Meth. 105, 103-107 (1972)

of the collimator and shadow rod in front of the counter, reduce front- end- and side-wall effects and also prevent neutron transmission of the ceramic insulators of the anode wire.

Two runs, with gains of nominally 100 and 20 were needed to cover the energy range from 80 keV to 2 MeV. Each run was made in conventional one-dimensional time of flight analysis (time resolution of the detector device is 120 ns and the lowest lower level discriminator used so far corresponds to 24.4 keV neutron energy) and also in two-dimensional analysis of pulse height V and time of flight t . The data acquisition system is a General Automation 'GA' computer linked with the system controller 'SYCON' to CBNM's IBM 370 Central Computer. A user oriented programme for multiparameter analysis called MUP 2, was written and tested. This system was used to acquire V in 128 channels and t in 128 channels. To increase the range of analysis, both variables have means for channel compression or so-called accordions. A typical accordion setting on V was 64 channels of width "one", followed by 32 channels of width "two" and finally 32 channels of width "four". Similar accordion settings were used for the time, typically: 64 channels of 160 ns, 32 of 320 ns, and 32 of 640 ns. Initial delay was chosen to get the time analysis in an energy range with satisfactory energy resolution and appropriate counting rate and at the same time appropriate gain settings to get a pulse height analysis of neutron energy in less than 256 channels or less than 128 after compression.

A computer programme 'TRITON' was written to adapt the data to the existing plotting programme 'TRICE': removal of the accordions on two variables, provision of a vector $X_i \sim V$ and a vector $Y_i \sim t$. In addition 'TRICE' was extended for plots of 32 x 32 matrix to 128 x 128 matrix.

A plot of a Vxt analysis of 128 x 128 channels with accordion in two variables is shown in Fig. 1.22. This figure displays a response function obtained at 33.5 keV neutron energy, carbon recoils can be observed in the pulse height distributions. The development of a dynamic discriminator both by software and hardware is completed. A detailed analysis and comparison of neutron obtained by one and two dimensional acquisition is in progress and a comparison of measured and calculated response functions for the peculiar geometry is planned. These investigations are part of CBNM's effort to determine fast neutron fluxes at the white source of the linac.

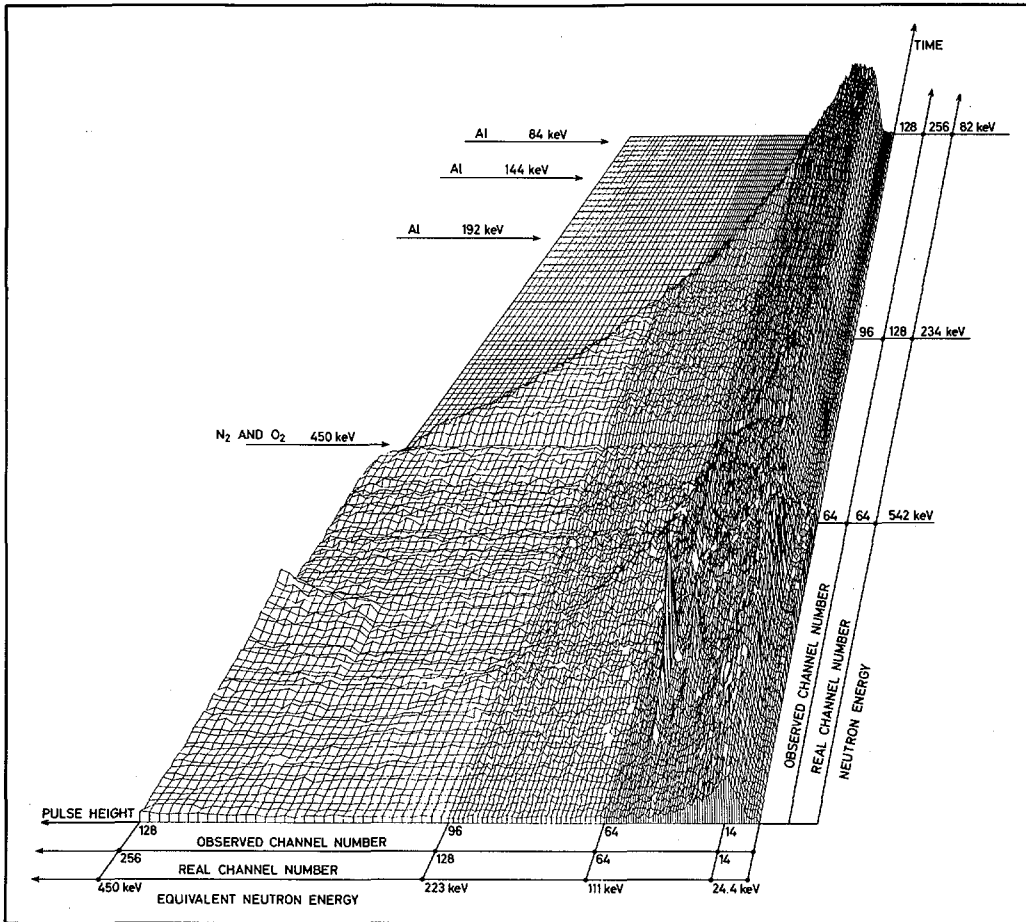


Figure 1.22 Two-dimensional analysis of pulse height and time of flight of a CH_4 filled proportional counter.

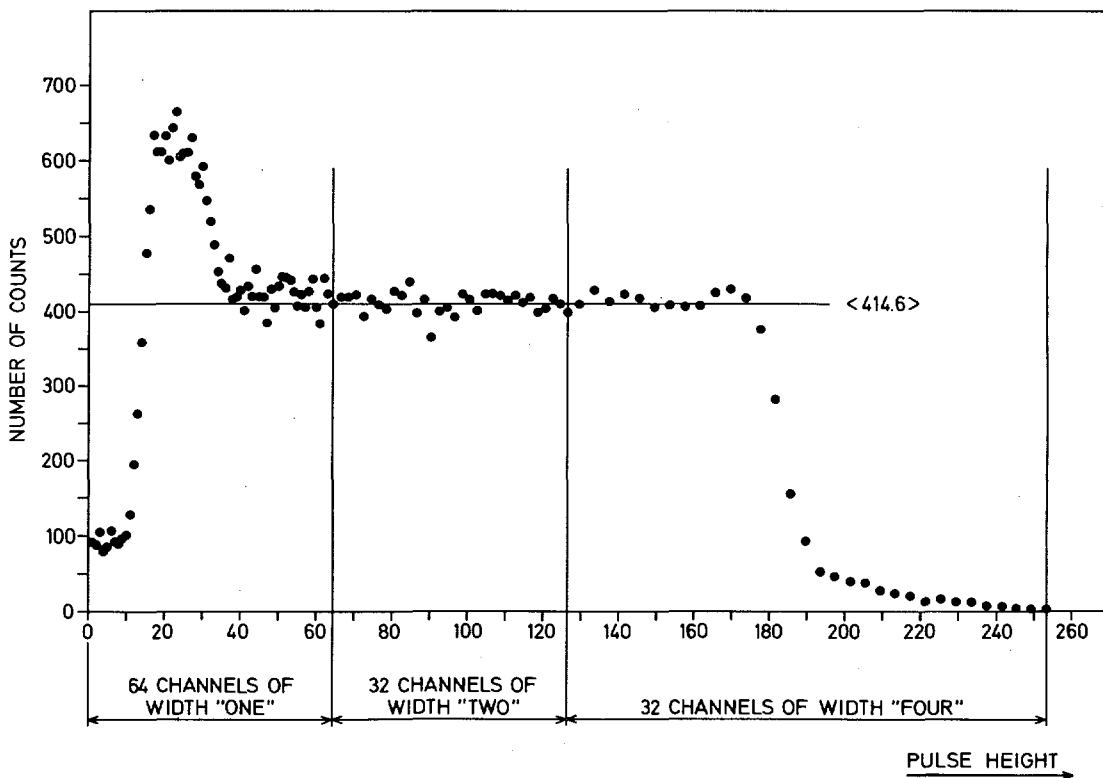


Figure 1.23 Pulse height spectrum of a CH_4 filled proportional counter irradiated with neutrons of $333.5 \text{ keV} \pm 4.5 \text{ keV}$. Number of counts are per $\Delta t = 320 \text{ ns}$, per $\Delta V = \text{"one"}$, per 75.600 sec with 9kW beampower.

2. NON-NEUTRON NUCLEAR DATA

2.1 Decay Studies

Decay of $^{93}\text{Nb}^m$

D. Reher, R. Vaninbroukx

The measurements for the determination of the half-life of $^{93}\text{Nb}^m$ have been continued using Si(Li) detectors. Four sources prepared from two different samples have been measured 21 times over a period of 3.5 years.

The mean value of the preliminary result is: $T_{1/2} = (15.9 \pm 1.0)\text{a}$. This value agrees well with the value of $(16.1 \pm 0.4)\text{a}$ communicated by R. Lloret⁽¹⁾.

Measurements of internal conversion data in the $^{93}\text{Nb}^m$ decay have been carried out using a pressurized 4π proportional counter and LEXES, a Low Energy X-Ray and Electron Spectrometer. The sources were prepared using argon ion-beam sputtering of $^{93}\text{Nb}^m$ metal onto carbon foils of $15\text{-}20\ \mu\text{g}/\text{cm}^2$ thickness.

The self absorption of these sources was low enough to separate the K- and LM+ electron lines in the 4π proportional counter spectra (Fig. 2.1). Also the MN+ electron peak could be distinguished from the L-electron peak in the spectra measured with the open Si(Li) detector of LEXES (Fig. 2.2). Coincidence measurements between the K conversion electrons detected with the open Si(Li) and the KX rays detected with a high purity Ge detector were carried out. From all these measurements and the knowledge of the disintegration rate of the sources, determined by calibrated Si(Li) measurements, the internal conversion data given in Table 2.1 were deduced and compared with theoretical prediction of Rösels et al.⁽²⁾ for a pure M4 transition and $E_\gamma = 30.75\ \text{keV}$. All results are preliminary.

Decay of $^{103}\text{Rh}^m$

R. Vaninbroukx, W. Zehner

For the study of the reaction $^{103}\text{Rh}(n,n')$ at the Van de Graaff accelerator the $^{103}\text{Rh}^m$ disintegration rate of irradiated Rh samples (foils of 20 mm diameter and 0.1 mm thickness) had to be determined. Measurements of the emitted Rh KX rays were performed using two calibrated Si(Li) detectors each with a resolution of about 600 eV FWHM at 20 keV.

-
- (1) R. Lloret (CEN Grenoble), Private communication, January 1980
(2) F. Rösels, H.M. Fries, K. Alder, H.C. Pauli, Internal conversion coefficients for all atomic shells, Atomic Data and Nucl. Data Tables 21, 91 (1978)

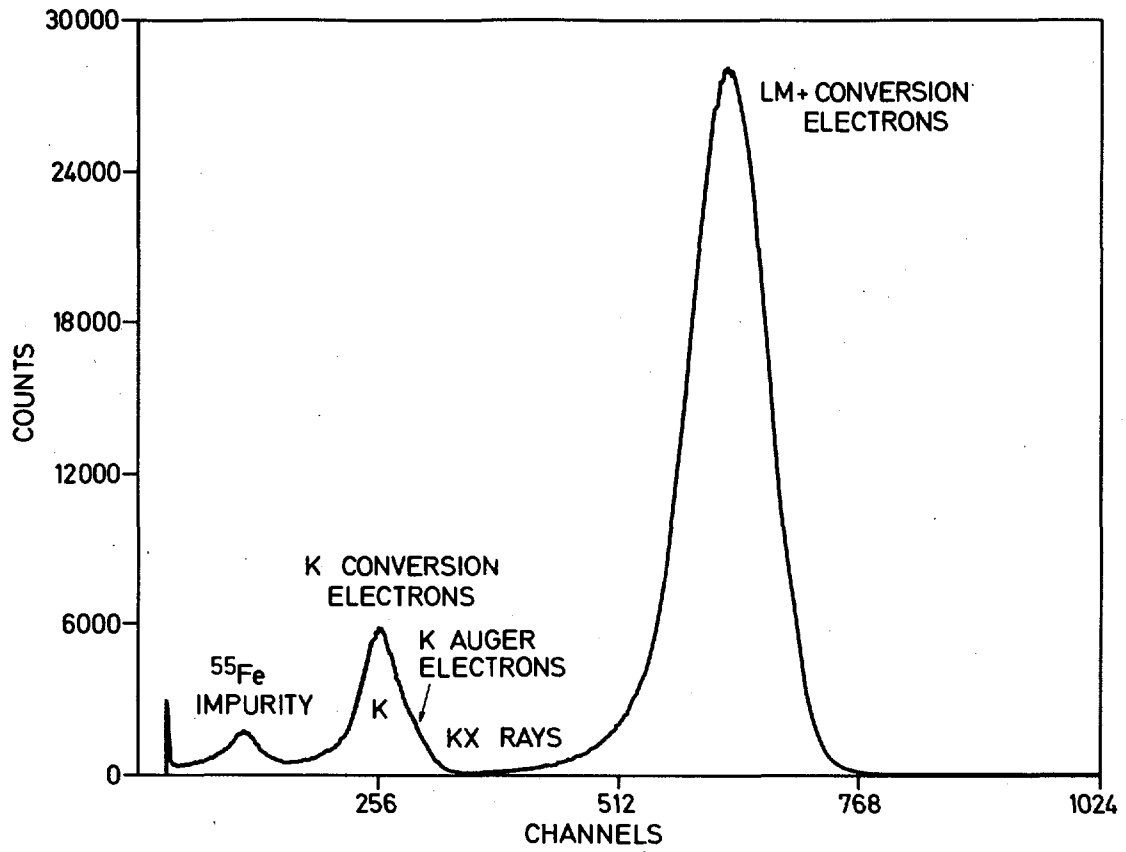


Figure 2.1 $^{93}\text{Nb}^m$ spectrum measured with a pressurized 4π proportional counter.

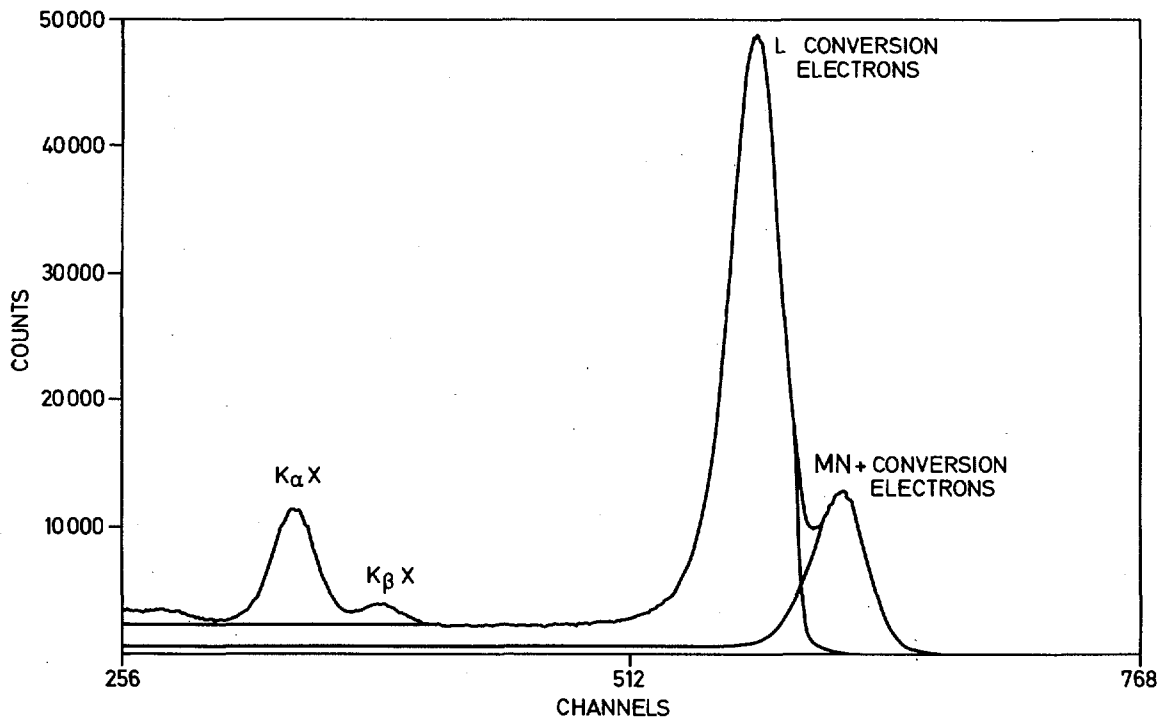


Figure 2.2 Spectrum of $^{93}\text{Nb}^m$ measured with an open Si(Li) detector.

TABLE 2.1.

Internal conversion data of $^{93}\text{Nb}^m$. Comparison of results with theoretical predictions of Rösler et al.

Quantity determined	Present results	Theoretical prediction of Rösler et al.
K/LM+ (a)	0.19 ± 0.02	0.171
K/L (a,c)	0.24 ± 0.03	0.214
L/MN+ (c)	3.8 ± 0.4	3.96
$a_K/a \approx \kappa_K$ (a)	0.16 ± 0.02	0.146
κ_K (a,b)	0.17 ± 0.02	0.146
κ_K (d,b)	0.15 ± 0.05	0.146
κ_{L+} (a,b)	0.85 ± 0.06	0.854
κ_L (a,b,c)	0.67 ± 0.09	0.683
κ_{MN+} (a,b,c)	0.18 ± 0.03	0.172

- (a) from the measurements with the 4π proportional counter,
- (b) from determination of the disintegration rate
- (c) from measurements with the open Si(Li) detector of LEXES,
- (d) from coincidence measurements with LEXES.

The Si(Li) detectors were calibrated for thin $^{103}\text{Rh}^m$ sources. $^{103}\text{Rh}^m$ was separated from ^{103}Pd (half-life 17 d) solutions in ion exchange columns. The most important correction in the determination of the activity of the Rh samples with a thickness of 0.1 mm ($\sim 120 \text{ mg/cm}^2$), is that for the self-absorption of the KX rays. Transmission measurements were performed using ^{103}Pd sources, emitting per decay about 0.8 Rh KX rays and less than 10^{-3} photons of higher energies. The sources were prepared on foils of 7 mg/cm^2 thickness. They were inserted at different positions in foil stacks of total thicknesses varying between 7 and 150 mg/cm^2 . Integration of the observed count rates over the total thickness of the stacks yields the mean count rate and, hence, the mean transmission for a foil of the corresponding thickness with uniformly distributed activity.

The results obtained in this way for the two detectors are given in Fig. 2.3. They are compared with a curve calculated from the formula $(1 - e^{-\mu d})/\mu d$, which in principle is only valid for small solid angles where the detected radiation passes perpendicularly the absorbing foil. The absorption coefficients $\mu(K_\alpha) = 15.3 \text{ cm}^2/\text{g}$ and $\mu(K_\beta) = 11.0 \text{ cm}^2/\text{g}$ for rhodium were taken from McMaster et al. (1).

The calculated mean transmission for $120 \text{ mg}/\text{cm}^2$ rhodium foils is 0.4735. The experimental values of 0.474 ± 0.003 and 0.456 ± 0.004 were used for the detection systems with $\Omega = 0.2$ and 0.4 sr , respectively.

The overall uncertainty of the detection efficiency corresponding to a 1σ confidence level was estimated from the individual uncertainties to be $\pm 1.2 \%$.

In the frame of this work some decay parameters of $^{103}\text{Rh}^m$, reported earlier (2), have been redetermined with better accuracies. The results are summarized in Table 2.2., where quoted uncertainties, corresponding to a 1σ confidence level, take into account random and systematic effects. The project is concluded and the results have been published (3).

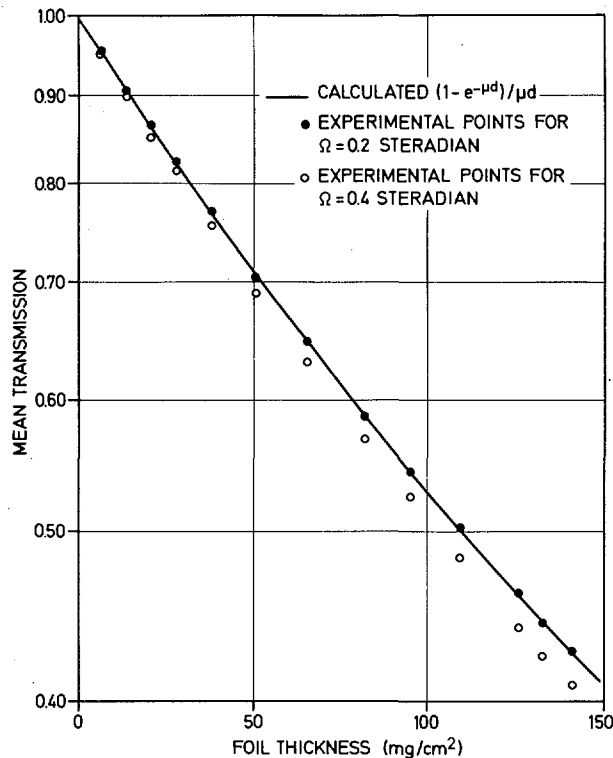


Figure 2.3 Calculated and measured mean transmission of the Rh KX rays emitted from $^{103}\text{Rh}^m$ uniformly distributed within rhodium foils.

- (1) W.H. McMaster, N.K. Delgrande, J.H. Mallett, J.H. Hubbel, "Compilation of X-ray cross sections", UCRL-50174, Sec.II, Rev. I. Lawrence Livermore Laboratory (1969)
- (2) R. Vaninbroux, "The use of liquid scintillation counting techniques for decay parameter studies of radionuclides decaying via low energy isomeric transitions", in C.T. Peng, D.L. Horrocks, and E.L. Alpen (Eds.), Liquid Scintillation Counting, Vol. 1 (Academic Press, Inc. New York, 1980), p. 143
- (3) A. Paulsen, R. Widera, R. Vaninbroux, H. Liskien, Cross-section measurement for the reaction $^{103}\text{Rh}(n,n')^{103m}\text{Rh}$, Nucl. Sci. Eng. 76, 331 (1980)

TABLE 2.2.
Decay parameters of $^{103}\text{Rh}^m$

Parameter		Result
Half-life	$T_{1/2}$	$(56.114 \pm 0.020) \text{ min}$
KX-ray emission probability	P_{KX}	$(8.43 \pm 0.04) \cdot 10^{-2}$
39.8 keV γ -ray emission probability	P_{γ}	$(7.2 \pm 0.2) \cdot 10^{-4}$

Decay of ^{133}Ba

H.H. Hansen, G. Grosse, D. Mouchel, R. Vaninbroukx

Spectra of internal conversion electrons especially of the low energy transitions of 81, and 161 keV in ^{133}Cs have been recorded with a magnetic β^- -spectrometer. The detection system used was a 5 mm thick plastic scintillator connected to a phototube with low noise characteristics. An experimental electron spectrum from the ^{137}Cs decay has been compared with the theoretical one as calculated from the corresponding Kurie plots. Below an electron energy of 130 keV a disagreement of more than 1 % between the two types of spectra has been found. A correction factor has been defined as the ratio of the theoretical and the experimental electron rate, $n(\text{theor})/n(\text{exp})$, and determined as a function of the electron energy. This correction factor has been applied to the experimental internal conversion electron spectrum of the low-energy transitions in ^{133}Cs .

For the 81 keV transition preliminary results which are mean values of 5 measurements are shown for the internal conversion ratios K/LM+, K/L, K/M+ and L/M+ in Table 2.3. The values are in good agreement with scarce experimental results found in the literature. The quoted uncertainties are standard deviations and do not include any systematic influences.

Spectra of internal conversion electrons of the 161 keV transition in ^{133}Cs were also evaluated. As the intensity of the 161 keV transition is very low long experimental runs were needed to obtain the K and LM+ internal conversion electron lines satisfactorily well separated from the underlying background. A preliminary value of $K/\text{LM+} = 3.87$ was calculated as a mean of 4 sets of measurements with a standard deviation of the mean of about $\pm 5\%$.

TABLE 2.3.

Preliminary results of internal conversion electron ratios for the 81 keV transition in ^{133}Cs

$\frac{K}{LM+} = 4.74 \pm 0.15$	$\frac{K}{MN+} = 21.1 \pm 0.9$
$\frac{K}{L} = 6.15 \pm 0.20$	$\frac{L}{MN+} = 3.43 \pm 0.17$

The measurements for the half-life determination have been continued. Three new sets of the photon spectrum emitted in the ^{133}Ba decay have been obtained from the Ge(Li) spectrometer experiment. For each run two different sources were used. In total the decay has been followed for a period of about 27 months. The preliminary mean value for the half-life obtained from 18 individual results is 10.58a with a standard deviation of the mean of $\pm 0.75\text{a}$. Similarly the experiment using three sources under five different geometrical conditions on the NaI(Tl) γ -ray spectrometer has been pursued. Up to now the ^{133}Ba decay has been observed during a period of about 5.5 years. The deduced half-life of $(10.54 \pm 0.15)\text{a}$ also has to be considered as preliminary.

Internal conversion ratios in the decay of ^{152}Eu

H.H. Hansen, D. Mouchel

Spectra of internal conversion electrons of the transitions of 244 keV (in ^{152}Sm following the EC-decay of ^{152}Eu) and of 344 keV (in ^{152}Gd following the β^- decay of ^{152}Eu) have been recorded with the magnetic β^- spectrometer. A 5 mm thick plastic scintillator coupled to a low-noise phototube was used as a detector.

An electron spectrum after subtraction of background and continuous β^- contribution is shown in Fig. 2.4. In the energy-region considered the deformation of measured spectra due to energy loss of the emitted electrons and due to electronic bias settings is less than 1 %.

The evaluation of the spectra is in progress and will result in values for the conversion ratios K/LM+.

Decay of ^{224}Ra

G. Bortels, D. Reher,
R. Vaninbroukx

For the Uranium Series Inter-comparison Project (USIP) for dating groundwaters by measurements of uranium and thorium isotope disequilibria, the relative α emission probability of the 5.45 MeV α transition to the excited level of 241 keV of ^{220}Rn in the ^{224}Ra decay is of relevance.

The emission probability of about 5 % is only known with an accuracy of 10 %. The 5.45 MeV α line is located under the 5.42 MeV main peak of ^{228}Th , the spike used by most of the laboratories of the USIP. The emission probability to the 241 keV level can be measured by α -particle spectrometry or by determining the γ -emission probability for the 241 keV photons and calculating then the α -emission probability taking into account the internal conversion coefficient. Both methods were applied. The nuclide ^{224}Ra belongs to the $^{232}\text{U} - ^{228}\text{Th}$ decay chain. The ^{224}Ra and the subsequent daughters in a ^{228}Th sample is in secular equilibrium after a period of 1 to 2 months. For the measurements we used ^{228}Th material which is more than 13 years old.

The γ -ray emission probability, $P_\gamma(241)$, of the 241.0 keV photons from the ^{224}Ra decay was determined using a calibrated pure Ge detector. It has also been determined relative to the rather well known emission probability $P_\gamma(239)$

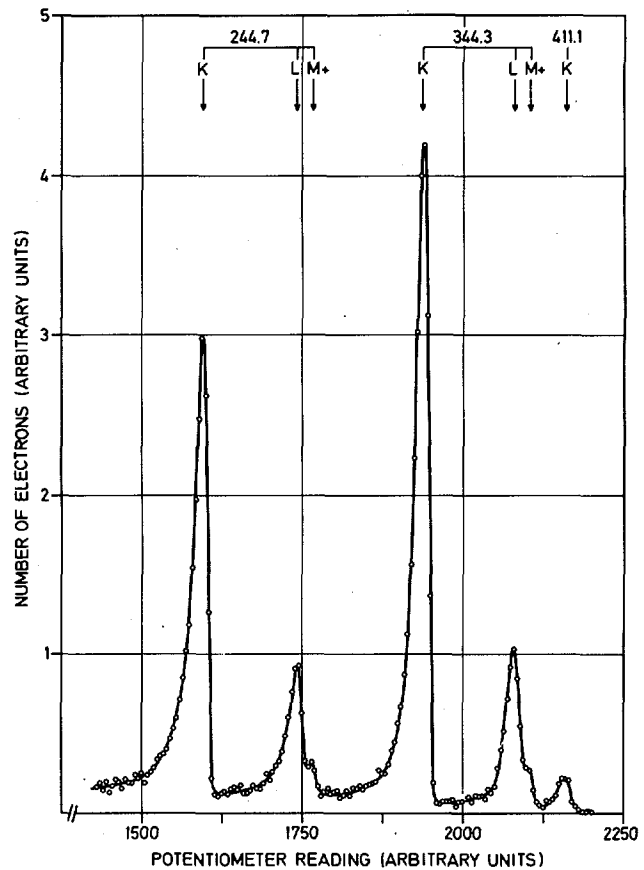


Figure 2.4 Number of electrons as a function of the electron momentum (proportional to the potentiometer reading of the β -spectrometer current supply). The groups of arrows show the positions of the conversion electron lines from different shells (K,L,M+) for three transitions in the decay of ^{152}Eu . The transition energies are indicated in keV.

of the 238.6 keV γ ray from the ^{212}Pb decay, which also belongs to the ^{228}Th decay chain. A typical γ -ray spectrum of $^{224}\text{Ra} - ^{212}\text{Pb}$ decays in the region around 240 keV is shown in Fig. 2.5.

The emission probability $P_\gamma(239)$ from the ^{212}Pb decay was also redetermined.

For the calculation of the α -emission probability $P_\alpha(241)$ of ^{224}Ra to the 241 keV level the total conversion coefficient for the 241 keV γ transition was obtained by interpolation of the values tabulated by Röseler et al. (1): $a_T = 0.282 \pm 0.007$.

The preliminary results of the measurements are:

$$\begin{aligned} P_\gamma(239) &= 0.440 \pm 0.014 \\ P_\gamma(241) &= 0.0425 \pm 0.0020 \\ P_\alpha(241) &= 0.054 \pm 0.003 \end{aligned}$$

Possible escape of small amounts of the ^{220}Rn from the source could perturb the equilibrium between ^{224}Ra and the ^{220}Rn daughters. Further experiments will solve this problem.

The ^{224}Ra sources for the α spectrometric measurements have been produced by collecting recoil atoms from the decay of a ^{228}Th source onto a stainless steel tray. Source strengths of $60\text{--}120 \text{ s}^{-1}$ in the ^{224}Ra peaks were obtained in this way. Measurements were carried out using two new 100 mm^2 premium grade surface barrier detectors at a solid angle of about 0.6 sr.

A typical spectrum is shown in Fig. 2.6.

The preliminary value for the α -transition probability to the 241 keV level ($E_\alpha = 5.45 \text{ MeV}$), obtained from the measured ratio of the two ^{224}Ra peaks, is:

$$P_\alpha(241) = 0.051 \pm 0.001.$$

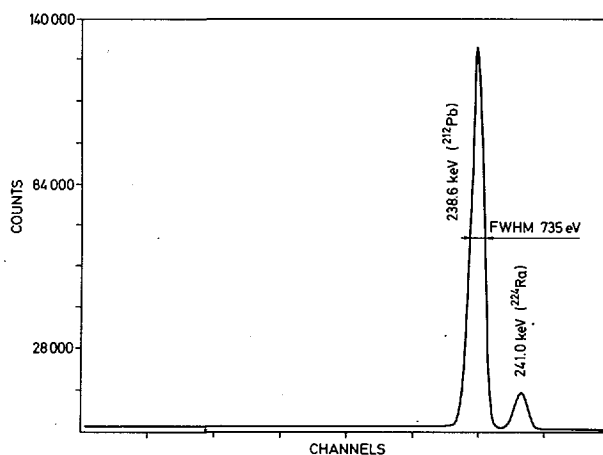


Figure 2.5 Partial γ -ray spectrum of $^{224}\text{Ra} - ^{212}\text{Pb}$ decays.

(1) F. Röseler, H.M. Fries, K. Alder, H.C. Pauli, Internal conversion coefficients for all atomic shells, Atomic Data and Nucl. Data Tables 21, 91 (1978)

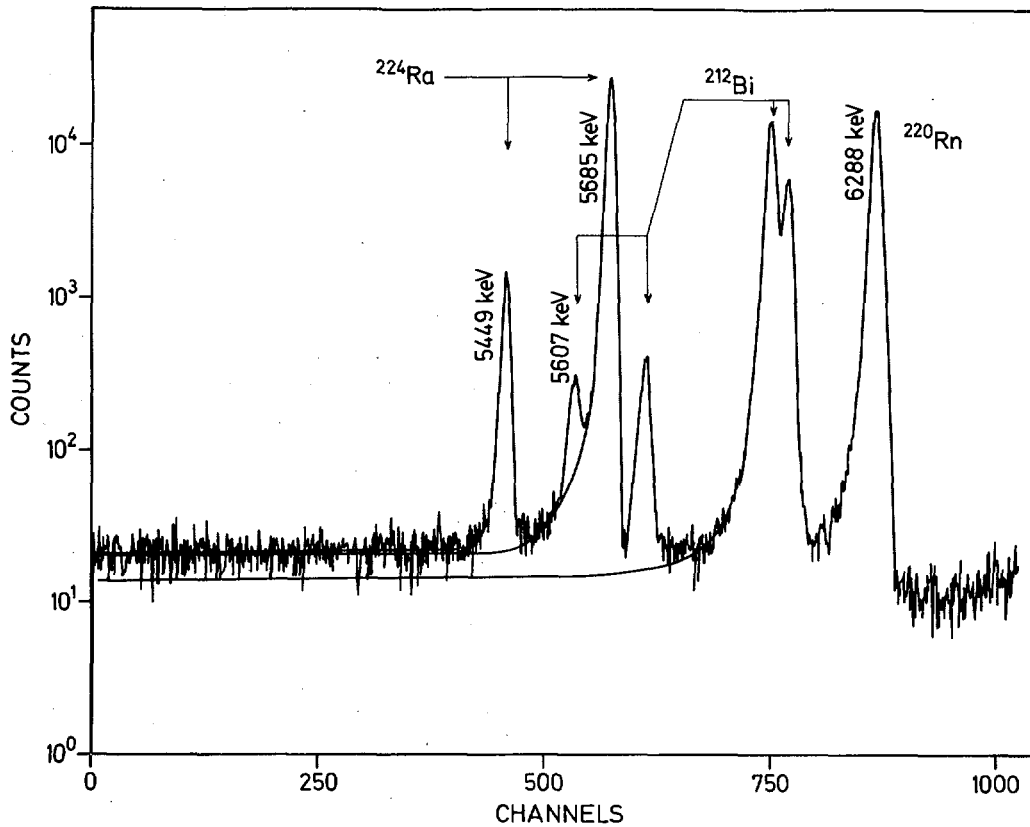


Figure 2.6 Alpha-particle spectrum of ^{224}Ra and daughters.

2.2 Half-life Determinations

Half-life of excited nuclear levels

A. Nylandsted Larsen, H.H. Hansen, D. Mouchel

The determination of the half-life of the first excited nuclear level of ^{181}Ta at 6.21 keV by the delayed coincidence technique has been finalized. A standard fast-slow delayed coincidence system consisting of two high-resolution Si(Li) detectors and a time-to-amplitude converter of the start-stop type was used in the experiments. Energy windows were set around the KX rays from the electron-capture decay of ^{181}W to ^{181}Ta and around the 6.21 keV γ rays. The KX rays and the 6.21 keV γ rays were used respectively to start and stop the time-to-amplitude converter. Much care was taken to make the ratio between true and accidental events as high as possible and to study the influence of the accidental events on the extracted half-life. The mean value of 18 measurements is found to be $T_{1/2} = (6.05 \pm 0.12)\mu\text{s}$.

The uncertainty quoted corresponds to the 1σ confidence level and takes into account both random (0.7 %) and systematic (1.3 %) effects. A paper has been accepted for publication in Z. Physik (1).

Half-lives of ^{57}Co , ^{103}Ru , $^{103}\text{Rh}^m$, ^{103}Pd , and ^{109}Cd

R. Vaninbroukx, G. Grosse, W. Zehner

During the last years the radionuclides ^{57}Co , ^{103}Ru , $^{103}\text{Rh}^m$, ^{103}Pd , and ^{109}Cd have been extensively used at CBNM for γ -ray detector efficiency calibration. In addition $^{103}\text{Rh}^m$ is of interest for the determination of the $^{103}\text{Rh}(n,n')$ cross section. From those measurements using NaI(Tl) and Si(Li) detectors accurate half-life values could be deduced. These measurements have now been concluded. The final results for the half-lives are summarized in Table 2.4. They have been submitted for publication.

TABLE 2.4.

Final results for the half-lives of various radionuclides

Nuclide	Sample	Detector	Number of individual series	Period of observation in half-lives	Half-life \pm standard error	Weighted mean and overall uncertainty(*)
^{57}Co	1	NaI(Tl)	11	3.5	(271.89 \pm 0.02)d	(271.90 \pm 0.09)d
	2	NaI(Tl)	6	1.3	(271.86 \pm 0.06)d	
	2	Si(Li)	6	3.2	(271.94 \pm 0.25)d	
	3	NaI(Tl)	6	3.0	(271.92 \pm 0.03)d	
^{103}Ru	1	NaI(Tl)	12	3.3	(39.260 \pm 0.003)d	(39.260 \pm 0.020)d
	2	NaI(Tl)	12	3.3	(39.259 \pm 0.004)d	
$^{103}\text{Rh}^m$	1	NaI(Tl)	3	2.1	(56.107 \pm 0.021)m	(56.114 \pm 0.020)m
	2	NaI(Tl)	4	3.0	(56.116 \pm 0.012)m	
^{103}Pd	1	NaI(Tl)	2	2.0	(17.030 \pm 0.028)d	(16.991 \pm 0.019)d
	1	Si(Li)	6	2.9	(16.992 \pm 0.012)d	
	2	NaI(Tl)	9	3.2	(16.991 \pm 0.010)d	
	2	Si(Li)	3	2.6	(16.963 \pm 0.030)d	
^{109}Cd	1	Si(Li)	4	1.9	(461.61 \pm 0.23)d	(461.90 \pm 0.30)d
	2	NaI(Tl)	8	1.1	(461.43 \pm 0.25)d	
	3	NaI(Tl)	6	2.1	(462.10 \pm 0.11)d	

(*) The overall uncertainty, corresponding to a 1σ level, takes into account random and systematic uncertainties.

(1) D. Mouchel, A. Nylansted Larsen, H.H. Hansen, Half-life of the 6.21 keV level in ^{181}Ta , Z. Physik, in press

2.3 Compilations and Evaluations

Internal conversion data

H.H. Hansen

Final proof reading was performed of the tables and the reference listing of the compilation of the experimental internal conversion data for $Z \leq 60$. The report is in press ⁽¹⁾. The data-file will be updated in the future. Some important internal conversion coefficients and ratios are being evaluated.

Fluorescence yields

W. Bambynek

The evaluation of X-ray fluorescence yields published later than 1972 was continued. Reliable values from new measurements were selected. They will be included in a new set of data to be compared with recent relativistic predictions ⁽²⁾.

Decay data of actinides

R. Vaninbrouckx

A review paper on the status of nuclear decay data of actinides has been presented at the Second Technical Meeting on the Nuclear Transmutation of Actinides, Ispra, 21-24 April, 1980 ⁽³⁾. Furthermore, a report was given on recent IAEA meetings concerning the Coordinated Research Programme on the Measurements and Evaluation of Transactinium Isotope Decay Data in which CBNM is participating.

-
- (1) H.H. Hansen, Compilation of experimental values of internal conversion coefficients and ratios for nuclei with $Z \leq 60$, Physik Daten/Physics Data 17-1 (1981)
 - (2) M.H. Chen, B. Crasemann, Hans Mark, Relativistic K-shell Auger rates, level widths, and fluorescence yields, Phys. Rev. A 21, 436 (1980)
 - (3) R. Vaninbrouckx, Some observations on the status of nuclear decay data of actinides" in W. Hage (ed.), Proceedings Second Technical Meeting on the Nuclear Transmutations of Actinides, April 21-24, 1980, Ispra, (Commission of the European Communities, 1980)

Request list non-neutron nuclear data

W. Bambynek

This survey of the requirement of users of non-neutron nuclear data was carried out in an attempt to support the activity of the International Committee for Radionuclide Metrology (ICRM) Working Group Non-Neutron Nuclear Data. It includes mainly information on radionuclide decay scheme parameters and some atomic data ⁽¹⁾.

Most of the requests were received from ICRM members. Additional information was found in the reports of some IAEA advisory group meetings, such as the

- IAEA Consultants Meeting on Integral Cross Section Measurements in Standard Neutron Fields (1977),
- Second IAEA Advisory Group Meeting on Fission Product Nuclear Data (1977),
- IAEA Advisory Group Meeting on Transactinium Isotope Nuclear Data (1979).

Furthermore, the World Request List for Nuclear Data 79/80 which mainly contains neutron data requests, was consulted too.

Information that came to the compiler's knowledge before 1 March 1980 was taken into account.

2.4 Satellite Peaks in High Resolution Alpha Spectrometry and their Use in Determining the Energy Loss of Recoiling Nuclei of the ²²⁸Th Series to Electronic Processes in Silicon

A. Nylandsted Larsen, G. Bortels, B. Denecke

In high resolution α -particle spectra from decay chain members, measured with Si surface barrier (SB) detectors, satellite peaks are observed at the high energy side of some α peaks. This effect is enhanced in decay series with α emitters with relatively short half-lives. The origin of the satellite peaks has been investigated using two SB detectors on which recoiling daughter-nuclei from the decay of ²²⁸Th had been collected.

A typical spectrum taken with a SB detector with a 20 $\mu\text{g}/\text{cm}^2$ Au layer is shown in Fig. 2.7. Here the α peaks are accompanied by satellite peaks indicated by S. It can be shown that these satellite peaks stem from alpha decay of daughter-nuclei which have penetrated through the Au surface-barrier layer of the detector and into the Si crystal.

(1) W. Bambynek, The ICRM non-neutron nuclear data request list, EUR 6836 EN and ICRM-D-1 (1980)

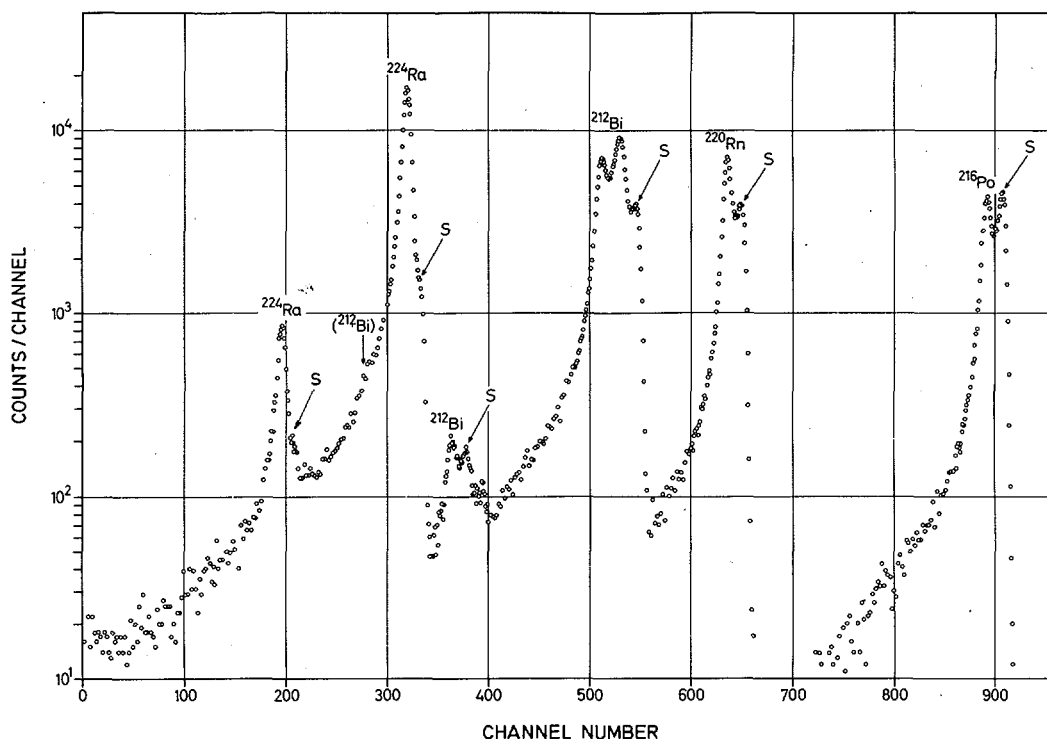


Figure 2.7 Alpha-particle spectrum from ²²⁸Th daughters recoil implanted into a 100 mm² silicon SB detector with 20 μg/cm² Au surface-barrier thickness.

When these nuclei decay, the emitted alpha particle and the recoiling daughter-nucleus will be detected simultaneously. This gives rise to a peak, shifted to a higher energy relative to the main alpha peak by an amount equal to the energy ΔT lost in ionization processes during the slowing-down of the recoiling nuclei in Si. These energies have been determined for recoiling nuclei of the ²²⁸Th decay series in Si. Excellent agreement is found between the two sets of ΔT values given in columns 3 and 4 of Table 2.5 for the two detectors. Mean values, $\overline{\Delta T}$, and fractional energy differences, $\overline{\Delta T}/T_D$ where T_D is the recoil energy, have been calculated and are given in columns 5 and 6, respectively. Theoretical predictions of the energy loss in electronic processes during the slowing down of the recoiling atoms in Si, η , and of the fractional energy loss η/T_D are given in columns 7 and 8, respectively. These have been calculated by Thomsen ⁽¹⁾ based on the theory of Lindhard et al. ⁽²⁾. The trend of the $\overline{\Delta T}$ values is very well described by the theory, however, the $\overline{\Delta T}$ values are 30-40 % lower than the theoretical predictions. A paper has been prepared for publication.

(1) P.B. Thomsen, Private communication, 1980

(2) J. Lindhard, V. Nielsen, M. Scharff, P.V. Thomsen, Integral equations governing radiation effects, Mat. Fys. Medd. Dan. Vid. Selsk. 33, 110.10 (1963)

TABLE 2.5.

Results of the determination of the energy loss in electronic processes in Si, ΔT , for the different recoiling daughter nuclei and for two detectors used. The theoretical predictions, η , by Thomsen are based on the theory of Lindhard et al.

Transition	Recoil Energy T_D (keV)	20 $\mu\text{g}/\text{cm}^2$ Au sur-	40 $\mu\text{g}/\text{cm}^2$ Au sur-	Mean values		Predictions of	
		face barrier layer ΔT (keV)	face barrier layer ΔT (keV)	ΔT (keV)	$\Delta T/T_D$	η (keV)	η/T_D
$^{224}\text{Ra} \rightarrow ^{220}\text{Rn}$	104	19 \pm 4	19 \pm 4	19 \pm 4	0.18 \pm 0.04	31.0	0.298
$^{220}\text{Rn} \rightarrow ^{216}\text{Po}$	117	22 \pm 2	24 \pm 2	23 \pm 2	0.20 \pm 0.02	35.5	0.303
$^{216}\text{Po} \rightarrow ^{212}\text{Pb}$	128	25 \pm 2	27 \pm 2	26 \pm 2	0.20 \pm 0.02	39.5	0.309
$^{212}\text{Bi} \rightarrow ^{208}\text{Tl}$	110	23 \pm 4	-	23 \pm 4	0.20 \pm 0.03	33.8	0.307
$^{212}\text{Po} \rightarrow ^{208}\text{Pb}$	169	38 \pm 3	39 \pm 3	39 \pm 3	0.23 \pm 0.02	54.0	0.320

2.5 Improvement of Measurement and Source Preparation Techniques

Low-energy X-ray standards

A. Kacperek, W. Bambynek, D. Reher

Quantitative measurement of the low energy X-rays with Si(Li) detectors is hampered by lack of suitable calibration sources. To calibrate a detector in this energy region a set of X-ray standards of defined energies and known source strength of about 10^6 to 10^7 s^{-1} is required. The final uncertainty on the calibration of these sources should be better than 5 %. Generally the available methods do not yield accuracies better than 10 % at photon energies below 5 keV. A method has been developed to prepare and standardize sources which would be simple to use for the calibration of solid state detectors at energies below 4 keV and which should be capable for higher accuracy. It is based on fluorescence excitation of elemental foils of low atomic number by a suitable X- or γ -ray source which is evaporated, in a well defined area of 3 or 5 mm diameter, directly onto the foil. In this way a physically robust and compact ensemble can be supplied. The standardization is done by a defined solid angle flow proportional counter. The excited X rays of Al, and also P, S and Cl were easily measured; less well were the Ca KX rays.

In Fig. 2.8 these were compared with spectra measured with a Si(Li) detector. Due to the absorption behaviour of these low-energy X rays there is an anisotropy which becomes more prominent for larger solid angles. Consequently, besides the source strength for X rays emitted perpendicular to the source plane, a curve of the anisotropy factor versus the solid angle or its cone semi-angle has to be determined and supplied to the user. The making and standardization of an Al KX-ray source ($E = 1.5$ keV) with an uncertainty of 3 % has been achieved.

A paper ⁽¹⁾ describing the preparation and calibration techniques for detector-efficiency calibration sources at photon energies below 4 keV has been presented at the International Conference on X-Ray Processes and Inner-Shell Ionization, Stirling, U.K.

The quantitative measurement of Al KX-ray sources has been improved. The main areas of endeavour have been:

- 1) the measurement of "source anisotropy", i.e. the change in response using different solid angles, and different angles of source emission;
- 2) the reduction of low-energy electronic noise; tests have been performed to compromise between noise and spectral resolution;
- 3) the modification of the flow proportional counter to reduce continuum background originating from higher energy photons;
- 4) efforts are being made to determine the absolute peak area of low energy X-rays, in particular Al KX-rays, situated on a relatively high background continuum.

4 π β - γ coincidence technique

A. Nylandsted Larsen, E. Celen

Measurements of the ⁶⁵Zn disintegration rate with a 4 π β - γ coincidence technique have been continued. It can be shown theoretically that a straightforward extrapolation of N_{XA} versus $1 - \epsilon_{XA}$ to $1 - \epsilon_{XA} = 0$, where N_{XA} is the count rate of the proportional counter due to electron capture events and ϵ_{XA} is the efficiency of the proportional counter for detection of such events, leads to an overestimation of the disintegration rate, N_0 , of the source by about 0.3 %. Linearity of the extrapolation curve and possible influences on this linearity by different energy discriminations in the proportional counter chain are under investigation.

(1) A. Kacperek, W. Bambynek, D. Reher, Detector efficiency calibration sources at photon energies below 4 keV, International Conference on X-Ray Processes and Inner-Shell Ionization, Stirling, U.K., 25-29 August 1980, in press

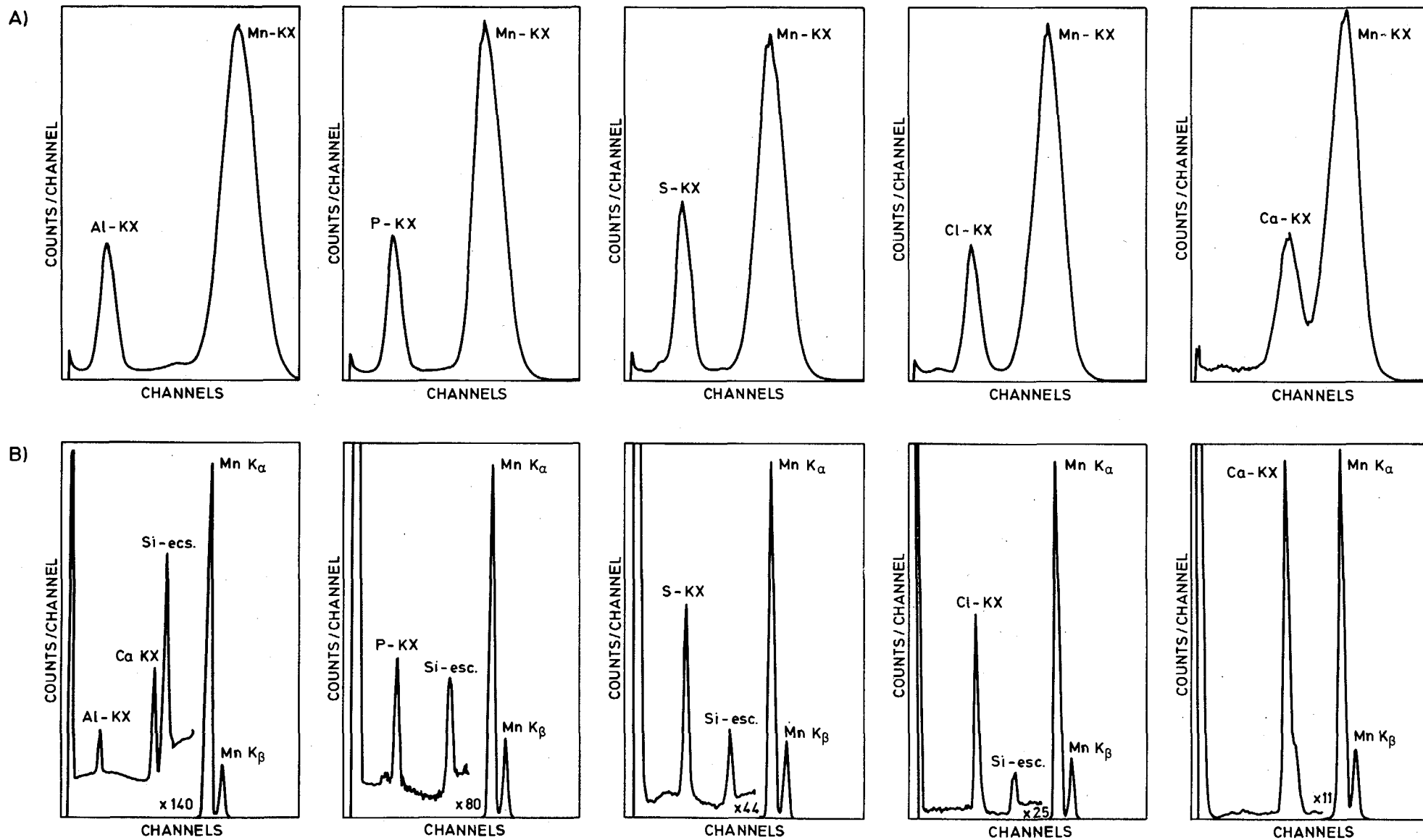


Figure 2.8 KX-ray spectra measured with A) flow proportional counter, B) Si(Li) detector.

Source preparation

W. Oldenhof, W. Zehner

The preparation of thin, homogeneous sources with low self-absorption is important for accurate measurements of radionuclides. An improvement for quantitative source preparation is the utilization of the freeze-drying process. This technique was made available and is under test now. Additionally, a method described by Lowenthal and Wyllie ⁽¹⁾ was set up and first experiments have been started. An essential point is that the ion exchange resins particles, which have to be suspended in ethanol and electro-sprayed onto metallized source backing, are ground finely to at least 0.2 μm . About 200 radioactive sources (⁵⁵Fe, ⁵⁷Co, ⁶⁰Co, ⁶⁵Zn, ⁹³Nb^m, ¹⁰³Rh^m, ¹²¹Sn, ¹³³Ba, ¹³⁷Cs, ¹³⁹Ce, ¹⁴¹Ce, ¹⁸¹W, ²²⁸Th) have been prepared by various techniques on Vyns, Formvar and carbon foils. About 250 supporting foils (Vyns, Formvar, carbon) have been made.

Niobium dosimetry intercomparison

D. Reher, R. Vaninbrouckx

CBNM participated in an interlaboratory niobium dosimetry comparison together with SCK-CEN Mol, AEE Winfrith, CEN Grenoble, GKSS Geesthacht, HEDL Hanford, KFA Jülich, and KWU Erlangen which was organized by SCK-CEN Mol.

We received four Nb dosimeters. Two of them have been irradiated in the fast breeder reactor EBR II at HEDL and two in the reactor BR 2 at SCK-CEN. The task was to determine the ⁹³Nb^m activity of these dosimeters generated by the ⁹³Nb(n,n')⁹³Nb^m reaction. Impurity determinations carried out with a calibrated Ge(Li) spectrometer showed, that the ¹⁸²Ta/⁹³Nb^m activity ratio varied between 0.03 % and 63.4 % whereas the sum of all other impurities relative to the ⁹³Nb^m activity varied from 0.2 % to 3.3 %. The dosimeters were dissolved in a mixture of concentrated HF and HNO₃. Drop evaporation sources were prepared from these solutions as well as liquid scintillation cocktails. From the drop sources the KX-ray intensity was derived by spectrometry with two calibrated Si(Li) detectors. Using $P_{KX} = \kappa K^{\omega_K} = 0.116 \pm 0.004$ the disintegration rate N_0 could be derived by $N_0 = N_{KX} / (P_{KX} \cdot \epsilon_{KX})$. From the liquid scintillation measurements N_0 was derived directly from the spectra. A summary of the results is given in Table 2.6.

(1) G.C. Lowenthal, H.A. Wyllie, Thin 4 π sources on electro-sprayed ion exchange resin for radioactivity standardization, Int. J. Appl. Radiat. Isotopes 24, 415 (1973)

TABLE 2.6.
Summary of the results of the $^{93}\text{Nb}^m$ activity determination

Dosimeter Nr.	8	1	SA/45-3	SA/46-2
Reactor/Run	BR2 7/78	BR2 7/78	EBR II 97	EBR II 97
Position in Reactor	+ 50 mm	- 150 mm	0 cm	- 15.4 cm
Manufacturer of Nb	MPI	GOODF	KAW	KAW
Masses (μg)	999	741	824	746
Impurity $^{182}\text{Ta}/^{93}\text{Nb}^m$	0.0003	0.0430	0.0070	0.6340
Impurity oth./ $^{93}\text{Nb}^m$	0.0186	0.0231	0.0024	0.0326
Activity (MBq)	0.749	0.545	2.365	0.191
Rel.Activ.(MBq/mg)	0.750	0.735	2.870	0.256
Rel.Uncertainty(1σ)%	1.1	0.7	1.1	2.0

Calibration of a $^{93}\text{Nb}^m$ solution and of $^{93}\text{Nb}^m$ sources

D. Reher, R. Vaninbroukx

On request of the Physikalisch-Technische Bundesanstalt (PTB), Braunschweig, 2.6 ml of a $^{93}\text{Nb}^m$ solution and four solid sources were calibrated to an accuracy of 1.3 % (1σ confidence level) at the reference date. Niobium is dissolved in a mixture of 2M HNO_3 + 1M HF. This precludes the use of glass or quartz bottles to contain the solution. Several types of plastic containers were tested (PE, PVC, PTFE) but with all of them weight-loss or -gain was observed with time, depending on the HF concentration.

The solution to be calibrated was sealed in a polyethylene pycnometer and its mass was controlled over a one month period. A mean weight loss of $(146 \pm 51)\mu\text{g}$ per day was observed. The rather high uncertainty of this value is correlated with temperature changes in the weighing room.

The outside surface of the pycnometer was controlled for contamination but no activity has passed the wall. Hence, the specific activity of the calibrated solution has not only to be corrected for decay (adopted value: $T_{1/2}(^{93}\text{Nb}^m) = (16.0 \pm 0.5)\text{a}$) but also for the mass-loss of 2 % per year. It is not known whether this correction is linear for periods longer than one month. Hence, if the accuracy of the calibrations of less than 2 % is to be maintained a recalibration of the solution after three months will be necessary.

2.6 Programme-linked Activities

Th/U ratio in spike solution

G. Bortels

The α -activity ratio of $^{228}\text{Th}/^{232}\text{U}$ in the spike used in the Uranium-Series Intercomparison Project (USIP), phase III, for dating geological samples has been measured. The spike solution had a ^{232}U activity concentration of about 1 kBq/ml. Drop-deposited (TEG) sources of about 60 Bq ^{232}U have been prepared on stainless steel trays. They have been covered with Vyns foils of either $70 \mu\text{g}/\text{cm}^2$ or $30 \mu\text{g}/\text{cm}^2$ thickness to prevent recoiling ^{224}Ra nuclei from being ejected when in vacuum.

Fig. 2.9 shows a typical spectrum measured with a 300 mm^2 Si-surface barrier detector. The shaded peak areas A and B indicate the uncorrected part of the spectrum considered for the determination of the $^{228}\text{Th}/^{232}\text{U}$ ratio. Two verified assumptions are made: (i) in the sources ^{228}Th and ^{224}Ra are in secular equilibrium, (ii) no recoiling ^{224}Ra nuclei are lost from the source. The number of counts from the major ^{224}Ra peak is obtained from area B in Fig. 2.9 after correction for all other contributions.

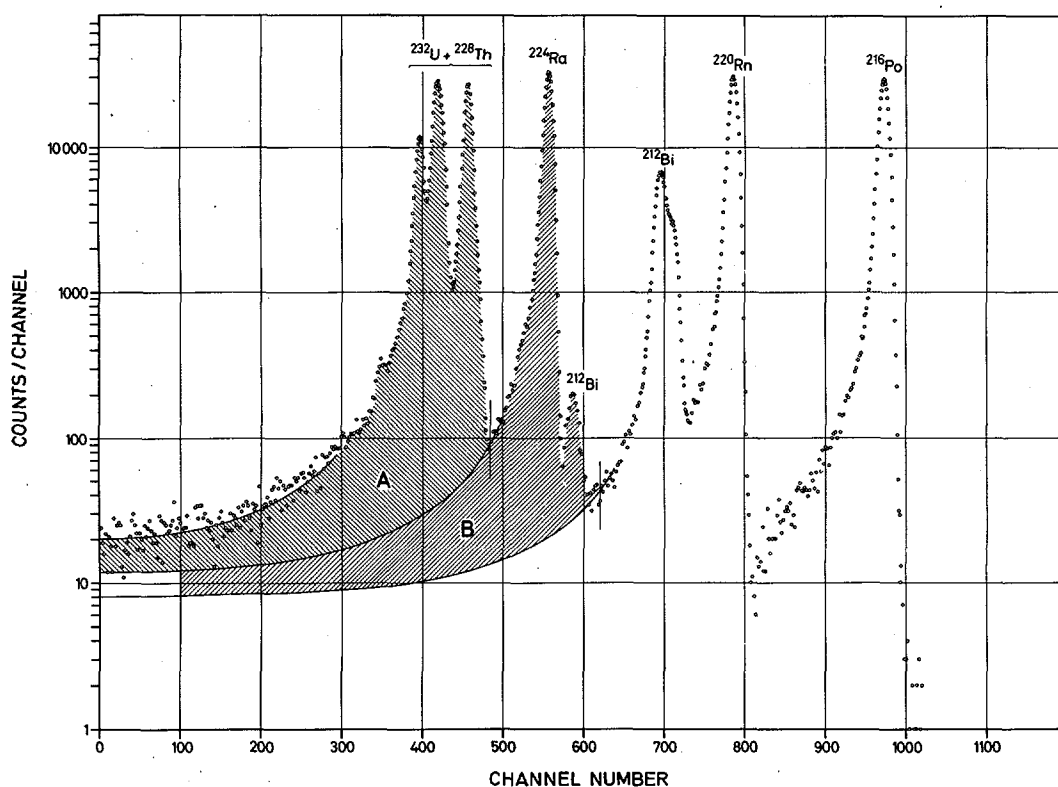


Figure 2.9 Alpha particle spectrum from a $^{228}\text{Th}/^{232}\text{U}$ spike solution. Drop-deposited (TEG) source covered with $30 \mu\text{g}/\text{cm}^2$ Vyns.

The results of the $^{228}\text{Th}/^{232}\text{U}$ alpha activity ratio determination dated from October 1st 1980 is: $^{228}\text{Th}/^{232}\text{U} = 0.978 \pm 0.011$.

The indicated uncertainty corresponding to a 1σ confidence level, is the linear sum of random (0.15 %) and systematic (0.9 %) contributions. The result has been communicated to the coordinator of USIP.

Radionuclide data acquisition system RNDAS

D. Reher

The first phase of the installation of a data acquisition system for radionuclide measurements is terminated. A PDP 11/34 minicomputer (32K word) together with some peripherals (Fig. 2.10) was installed.

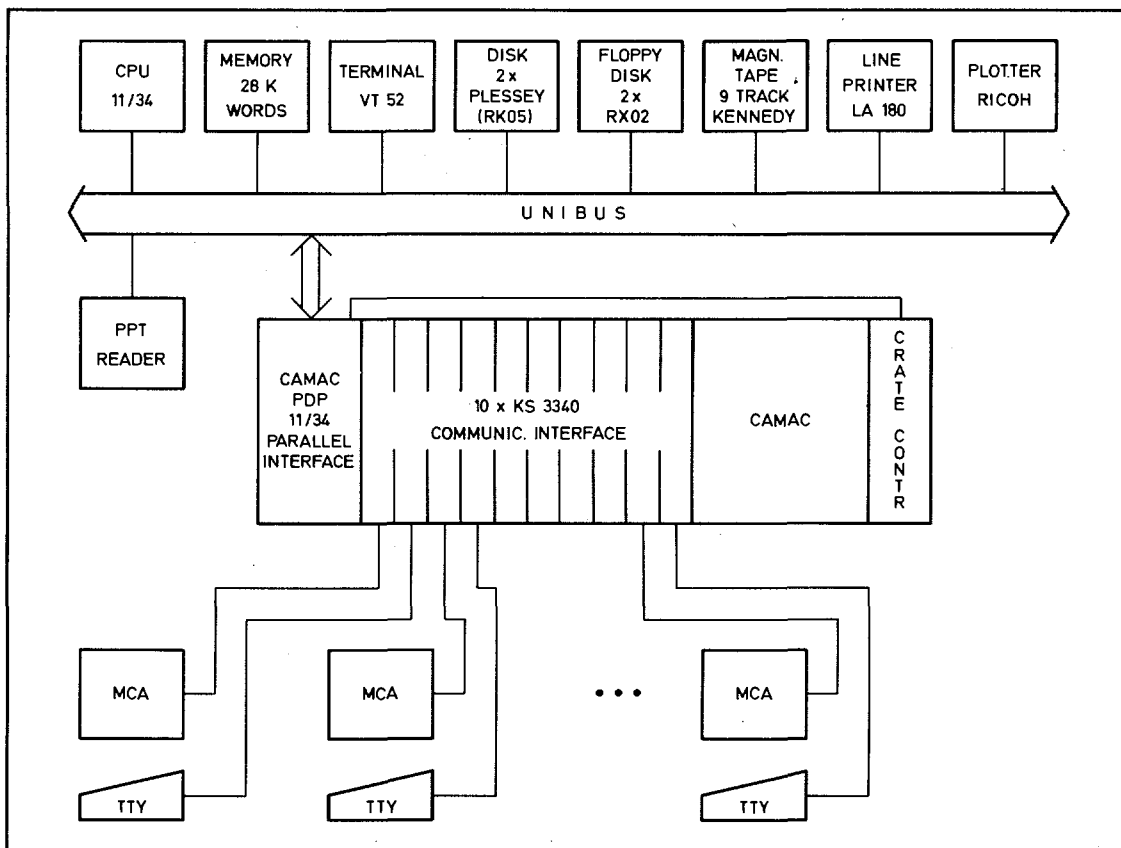


Figure 2.10 Block diagram of the first phase of RNDAS.

To the system a CAMAC station is coupled via an UNIBUS-CAMAC interface. Five multi-channel analyzers (MCA) of different types including their respective teletype printers in different rooms are connected to the CAMAC station (RS 232, 4800 baud).

The operating system used is RT-11 (foreground/background). In the foreground the system software, written to 90 % in FORTRAN IV, is controlling the data acquisition from the five multi-channel analyzers. The resident part of this programme together with the resident part of the operating system needs about 2/3 of the memory. In the background user programmes can be executed while data acquisition takes place. Programming languages available are FORTRAN IV, BASIC, MACRO and CLASS. Work on a package of routines and programmes for use in the background has started, and programmes to list and integrate spectra, read spectra from PPT, plot spectra, transfer spectra to magnetic tape, linear regression, spline interpolation, and other utilities are already available. The magnetic tape serves as a connection to the central computer facility of the institute.

LIST OF CBNM PUBLICATIONS

1. NUCLEAR DATA

1.1 Neutron Data

Publications in periodicals

- C. WAGEMANS, G. CODDENS, H. WEIGMANN, R. BARTHELEMY
Measurement of the $^{239}\text{Pu}(n,f)$ cross-section from thermal up to 30 keV neutron energy.
Ann. of Nucl. Energy, Vol 7, N° 9, p.495.
- C. BUDTZ-JØRGENSEN, H.-H. KNITTER
Neutron induced fission cross-section of ^{240}Pu in the energy range from 10 keV to 10 MeV.
Nucl. Sc. and Eng. (in publication).
- A. PAULSEN, H. LISKIEN, F. ARNOTTE, R. WIDERA
Measurement of (n,a) cross-sections on Cr, Fe and Ni in the 5 to 10 MeV neutron energy range.
Nucl. Sc. and Eng. (in publication).
- A. PAULSEN, R. WIDERA, R. VANINBROUKX, H. LISKIEN
Cross section measurement for the reaction $^{103}\text{Rh}(n,n')^{103}\text{Rh}^m$.
Nucl. Sci. Eng. 76, 331 (1980).

Conference Papers

- C. WAGEMANS, G. WEGENER-PENNING, H. WEIGMANN, R. BARTHELEMY
Proc. Conf. on Phys. and Chem. of Fission, IAEA, Vienna (1980) 143.
- E. CORNELIS, C. JUNGSMANN, L. MEWISSEN, F. POORTMANS
Total neutron cross section measurements on ^{54}Fe and ^{57}Fe .
Ibid. p. 159.
- A. BRUSEGAN, F. CORVI, G. ROHR, R. SHELLEY, T. van der VEEN
Neutron capture cross section measurement of ^{56}Fe .
Proc. Int. Conf. of Nucl. Cross Sections and Technology,
University of Tennessee, Knoxville, U.S.A., October 22-26, 1979
NBS Special Publication 594, 163
- P. STAVELOZ, E. CORNELIS, L. MEWISSEN, F. POORTMANS, G. ROHR,
R. SHELLEY, T. van der VEEN
Neutron resonance parameters for palladium isotopes.
Ibid. p. 315.

- J.M. SALOME, K.H. BÖCKHOFF
Performance improvements of the Geel Linac neutron source.
Ibid. p. 534.

- A. PAULSEN, H. LISKIEN, F. ARNOTTE, R. WIDERA
Measurement of (n,α) cross sections on Cr, Fe and Ni in the 5 to 10 MeV
neutron energy range.
Ibid. p. 844.

- C. WAGEMANS, G. CODDENS, A.J. DERUYTTER
 $^{235}\text{U}(n,f)$ cross section measurements and normalization problems.
Ibid. p. 261.

- P. STAVELOZ, E. CORNELIS, L. MEWISSEN, F. POORTMANS, G. ROHR,
R. SHELLEY, T. van der VEEN
Neutron resonance parameters for palladium isotopes.
Proceedings of the Specialists' Meeting on Neutron Cross Sections
of Fission Product Nuclei, Bologna, December 12-14, 1979, p. 53.

- G. ROHR, L. MAISANO, R. SHELLEY
Evaluation of average level spacing and S-wave strength function
performed for more than 240 nuclei.
Ibid. p. 197.

- G. ROHR, L. MAISANO, R. SHELLEY
The level density systematics applied to fission product nuclei.
Ibid. p. 207.

- G. ROHR
Pairing energies and single state densities studied by means of
level density systematics.
Int. Conf. on Nucl. Physics, Berkeley, August 1980, p. 765.

- H. WEIGMANN
Problems in the evaluation of fission cross section.
Int. Conf. on Evaluation Methods and Procedures, Brookhaven,
Sept. 1980.

- H. WEIGMANN
Theory and phenomenology of neutron induced fission cross sections.
Winter College on Nuclear Physics and Reactors, Trieste 1980,
IAEA, Vienna, to be published.

1.2 Non Neutron Data

Publications in periodicals

- A. NYLANDSTED LARSEN, D. MOUCHEL, H.H. HANSEN
Half-life of 23.87 keV level in ^{119}Sn .
Z. Physik A 294, 191 (1980).

- H.H. HANSEN
Compilation of experimental values of internal conversion coefficients and ratios for nuclei with $Z \leq 60$.
Physik Daten/Physics Data 17-1 (1981).

Conference Papers

- R. VANINBROUKX
"The use of liquid scintillation counting techniques for decay parameter studies of radionuclides decaying via low energy isomeric transitions", in Liquid Scintillation Counting, Vol. 1, p. 143, C.T. PENG, D.L. HORROCKS, and E.L. ALPEN, Eds., Academic Press, Inc., New York (1980).
- R. VANINBROUKX
"Some observations on the status of nuclear decay data of actinides", Proceedings Second Technical Meeting on the Nuclear Transmutations of Actinides, April 21-24, 1980, Ispra, Ed. W. HAGE, Commission of the European Communities (1980) p. 191.
- A. KACPEREK, W. BAMBYNEK, D. REHER
Detector efficiency calibration sources at photon energies below 4 keV. International Conference on X-Ray Processes and Inner-Shell Ionization, Stirling, U.K., 25-29 August 1980, in press.

EUR-Report

- W. BAMBYNEK
The ICRM non-neutron nuclear data request list.
EUR 6836 EN and UCRM-D-I (1980).

CINDA ENTRIES LIST

ELEMENT S A	QUANTITY	TYPE	ENERGY		DOCUMENTATION			LAB	COMMENTS	
			MIN	MAX	REF	VOL	PAGE			DATE
LI 006	N,TRITON	EXPT-PROG	10+1	50+5	INDC(EUR)	14	27	381	GEL	KNITTER+MEAS ANG DISTR.
LI 007	N,TRITON	EXPT-PROG	60+6	10+7	INDC(EUR)	14	14	381	GEL	LISKIEN+DIRECT DET OF TRITONS
C	TOTAL	EXPT-PROG	40+5	10+7	INDC(EUR)	14	26	381	GEL	CRAMETZ+VDG TOF TBD
SI 028	TOTAL	EXPT-PROG	40+5	10+7	INDC(EUR)	14	26	381	GEL	CRAMETZ+VDG TOF TBD
S	DIFF ELASTIC	EXPT-PROG	10+5	20+6	INDC(EUR)	14	26	381	GEL	JUNGMANN+11 ANGLES 26-154 DEG
K 040	N,PROTON	EXPT-PROG	20-2	70+4	INDC(EUR)	14	23	381	GEL	ASHGAR+ILL-HFR+LINAC TOF
K 040	N,ALPHA	EXPT-PROG	20-2	70+4	INDC(EUR)	14	23	381	GEL	ASHGAR+ILL-HFR+LINAC TOF
CR	N,ALPHA	EXPT-PROG	50+6	10+7	INDC(EUR)	14	11	381	GEL	PAULSEN+
CR 050	TOTAL	EXPT-PROG	50+2	15+5	INDC(EUR)	14	13	381	GEL	BRUSEGAN+
CR 050	TOTAL	EXPT-PROG	35+4	19+7	INDC(EUR)	14	13	381	GEL	CORNELIS+
CR 052	TOTAL	EXPT-PROG	50+2	15+5	INDC(EUR)	14	13	381	GEL	BRUSEGAN+
CR 052	TOTAL	EXPT-PROG	35+4	19+7	INDC(EUR)	14	13	381	GEL	CORNELIS+
CR 052	N,GAMMA	EXPT-PROG	NDG		INDC(EUR)	14	12	381	GEL	ALLEN+C6D6 DET LINAC TOF
CR 053	TOTAL	EXPT-PROG	50+2	15+5	INDC(EUR)	14	13	381	GEL	BRUSEGAN+
CR 053	TOTAL	EXPT-PROG	35+4	19+7	INDC(EUR)	14	13	381	GEL	CORNELIS+
FE	N,ALPHA	EXPT-PROG	50+6	10+7	INDC(EUR)	14	11	381	GEL	PAULSEN+
FE 054	TOTAL	EXPT-PROG	35+4	19+7	INDC(EUR)	14	13	381	GEL	CORNELIS+
FE 054	N,GAMMA	EXPT-PROG	NDG		INDC(EUR)	14	12	381	GEL	ALLEN+C6D6 DET LINAC TOF
FE 056	TOTAL	EXPT-PROG	35+4	19+7	INDC(EUR)	14	13	381	GEL	CORNELIS+
FE 057	TOTAL	EXPT-PROG	50+2	15+5	INDC(EUR)	14	13	381	GEL	BRUSEGAN+
FE 057	TOTAL	EXPT-PROG	35+4	19+7	INDC(EUR)	14	13	381	GEL	CORNELIS+
NI	N,ALPHA	EXPT-PROG	50+6	10+7	INDC(EUR)	14	11	381	GEL	PAULSEN+
SR 088	N,GAMMA	EXPT-PROG	20+2	60+5	INDC(EUR)	14	25	381	GEL	ALLEN.C6D6 DET LINAC TOF
RH 103	TOT INELASTC	EXPT-PROG	20+5	17+7	INDC(EUR)	14	14	381	GEL	PAULSEN+ACTIV ISOM,PUBL NUCL SCI ENG
PD 104	RESON PARAMS	EXPT-PROG	NDG		INDC(EUR)	14	14	381	GEL	STAVELOZ+
PD 105	RESON PARAMS	EXPT-PROG	NDG		INDC(EUR)	14	14	381	GEL	STAVELOZ+
PD 106	RESON PARAMS	EXPT-PROG	NDG		INDC(EUR)	14	14	381	GEL	STAVELOZ+
PD 108	RESON PARAMS	EXPT-PROG	NDG		INDC(EUR)	14	14	381	GEL	STAVELOZ+
PD 110	RESON PARAMS	EXPT-PROG	NDG		INDC(EUR)	14	14	381	GEL	STAVELOZ+
TH 232	TOTAL	EXPT-PROG	40+5	10+7	INDC(EUR)	14	26	381	GEL	CRAMETZ+VDG TOF TBD
U 233	N,FISSION	EXPT-PROG	25-2	10+5	INDC(EUR)	14	3	381	GEL	WAGEMANS+REL B10(N,A)
U 235	N,GAMMA	EXPT-PROG	10+3	10+5	INDC(EUR)	14	2	381	GEL	CALABRETTA+C6D6 DETECTORS TOF LINAC
U 235	FRAG SPECTRA	EXPT-PROG	25-2	10+0	INDC(EUR)	14	5	381	GEL	WAGEMANS+FRAG MASS+ENERG DISTR
PU 238	N,FISSION	EXPT-PROG	20+5	10+7	INDC(EUR)	14	5	381	GEL	KNITTER+REL U235(N,F)
PU 239	N,FISSION	EXPT-PROG	25-2	30+4	INDC(EUR)	14	6	381	GEL	WAGEMANS+PUBL ANN NUCL ENERG 7 495
PU 239	FRAG SPECTRA	EXPT-PROG	25-2	10+0	INDC(EUR)	14	5	381	GEL	WAGEMANS+FRAG MASS+ENERG DISTR
PU 240	N,FISSION	EXPT-PROG	10+4	10+7	INDC(EUR)	14	7	381	GEL	BUDTZ-JOERGENSEN+
PU 241	N,FISSION	EXPT-PROG	25-2	10+5	INDC(EUR)	14	3	381	GEL	WAGEMANS+REL B10(N,A)
PU 241	FRAG SPECTRA	EXPT-PROG	25-2		INDC(EUR)	14	9	381	GEL	ALLAERT+ FRAG MASS+ENERG DISTR
PU 242	N,FISSION	EXPT-PROG	50+5	50+6	INDC(EUR)	14	10	381	GEL	MOORE+
PU 242	FRAG SPECTRA	EXPT-PROG	SPON		INDC(EUR)	14	9	381	GEL	ALLAERT+ FRAG MASS+ENERG DISTR
PU 244	N,FISSION	EXPT-PROG	10+3	50+6	INDC(EUR)	14	10	381	GEL	MOORE+
PU 244	FRAG SPECTRA	EXPT-PROG	NDG		INDC(EUR)	14	10	381	GEL	MOORE+FRAG ANG DISTR IN PREP
AM 241	N,GAMMA	EXPT-PROG	50+0	10+5	INDC(EUR)	14	10	381	GEL	CORNELIS+TOF LINAC

Edited by G.H. DEBUS